A NEW APPROACH TO TIME-FREQUENCY LOCALIZED SIGNAL DESIGN

A THESIS

SUBMITTED TO THE DEPARTMENT OF ELECTRICAL AND

ELECTRONICS ENGINEERING

AND THE INSTITUTE OF ENGINEERING AND SCIENCES

OF BILKENT UNIVERSITY

IN PARTIAL FULFILLMENT OF THE REQUIREMENTS

FOR THE DEGREE OF

MASTER OF SCIENCE

By

Zafer Aydın

July 2001

I certify that I have read this thesis and that in my opinion it is fully adequate, in scope and in quality, as a thesis for the degree of Master of Science.

Assoc. Prof. Dr. Orhan Arıkan(Supervisor)

I certify that I have read this thesis and that in my opinion it is fully adequate, in scope and in quality, as a thesis for the degree of Master of Science.

Prof. Dr. Haldun Özaktaş

I certify that I have read this thesis and that in my opinion it is fully adequate, in scope and in quality, as a thesis for the degree of Master of Science.

Assist. Prof. Dr. Murat Alanyalı

Approved for the Institute of Engineering and Sciences:

Prof. Dr. Mehmet Baray
Director of Institute of Engineering and Sciences

ABSTRACT

A NEW APPROACH TO TIME-FREQUENCY LOCALIZED SIGNAL DESIGN

Zafer Aydın
M.S. in Electrical and Electronics Engineering
Supervisor: Assoc. Prof. Dr. Orhan Arıkan
July 2001

Design of signals in Wigner Domain has received considerable interest throughout the study of time-frequency signal synthesis. In commonly used design methods where the designer has to specify the desired Wigner distribution, the overall performance of the design is often adversely affected by the difficulty of representing the cross terms in the desired model. In this thesis we present a novel approach for the design of signals in Wigner Domain. In this method, the desired signal features in the time-frequency domain are specified in two stages. First the user is required to specify the spine which is the curve around which the energy of the desired signal is distributed. Once the spine of the desired signal is specified, the user is asked to specify the spread of the desired signal energy around the spine. In addition to this fundamentally new way of defining the time-frequency features of the desired signal, the actual synthesis of the signal is performed in a novel approach which is robust to the inadequately defined inner interference structure of the desired signal in the

Wigner domain. Once the spine of the desired signal is specified, a generalized warping function is obtained as a cascade of fractional Fourier transformation and warping. Then the actual signal synthesis takes place in the transformed signal domain where the inner interference terms of the signal are greatly reduced. After obtaining the designed signal in the transformed domain, it is transformed back to the original time domain providing the final result of the new signal synthesis technique.

Keywords: time-frequency, Wigner distribution, signal design, signal synthesis, spine, transformed signal domain, warped fractional domain

ÖZET

ZAMAN VE FREKANSTA LOKALİZE SİNYAL TASARIMINA YENİ BİR YAKLAŞIM

Zafer Aydın
Elektrik ve Elektronik Mühendisliği Bölümü Yüksek Lisans
Tez Yöneticisi: Doç. Dr. Orhan Arıkan
Temmuz 2001

Zaman-frekans sentez problemleri içerisinde en çok ilgi gören uğraş alanlarından biri Wigner düzleminde sinyal tasarımıdır. Yaygın olarak kullanılan tasarım yöntemlerinde tasarımcının arzulanan Wigner dagılımını baştan belirtmesi istenir. Arzulanan modelde kros terimlerin belirtilmesi zor olduğundan bu yöntemlerin genel performansı olumsuz yönde etkilenmektedir. Bu tezde Wigner düzleminde sinyal tasarımı ile ilgili yeni bir yöntem önermekteyiz. Bu yöntemde sinyalin zaman-frekans düzlemindeki arzulanan özellikleri iki aşamada belirlenir. Öncelikle kullanıcı omurgayı girer. Omurga, sinyalin enerjisinin etrafında dağılacağı eğridir. Omurga belirlendikten sonra, kullanıcıdan sinyalin omurga etrafında nasıl yayılacağını girmesi istenir. Arzulanan sinyalin zaman-frekans özellikleri temelde yepyeni bir şekilde belirlenmektedir. Bunun yanısıra asıl sinyal sentezi, Wigner düzleminde arzulanan sinyalin kros terimlerinin yeterince iyi girilememesinden kaynaklanan zorluklara karşı dayanıklı yeni bir yöntemle yapılmaktadır. Arzulanan sinyalin

omurgası belirlendikten sonra genellenmiş bükme fonksiyonu, kesirli Fourier dönüşümü ve bükme işleminin seri bileşimi olarak elde edilir. Daha sonra asıl sinyal sentezi, sinyalin kros terimlerinin oldukça azalmış olduğu dönüştürülmüş sinyal bölgesinde yapılır. Dönüştürülmüş sinyal bölgesinde tasarlanan sinyal, orijinal zaman bölgesine taşınarak yeni sinyal sentez tekniği tamamlanır.

Anahtar Kelimeler: zaman-frekans, Wigner dağılımı, sinyal tasarımı, sinyal sentezi, omurga, dönüştürülmüş sinyal bölgesi, bükülmüş kesirli bölge

ACKNOWLEDGMENTS

I would like to use this opportunity to express my deep gratitude to my supervisor Assoc. Prof. Dr. Orhan Arıkan for his guidance, suggestions and invaluable encouragement throughout the development of this thesis.

I would like to thank Prof. Dr. Haldun Özaktaş Assoc. Prof. Dr. Murat Alanyalı for reading and commenting on the thesis.

I express my special thanks to Kemal Özdemir for his effort, comments and great help.

Finally, many thanks to all of my close friends.

Contents

List of Figures

Chapter 1

INTRODUCTION

Signal Synthesis is one of the essential problems of Digital Signal Processing. In general, it refers to the design of signal samples that reflect the user specified attributes. Each system has its own characteristics and restrictions. It is the designer who should specify the desired qualities of the signal considering the domain that he operates on. Then it remains to select the algorithm or method that is acceptable in terms of accuracy and efficiency. In general there is no optimum method therefore algorithms are still developed that further compensate the need for better designs.

The common applications involve the synthesis of filter responses, synthesis of speech signals, synthesis of signals that have desired time-frequency properties, etc. In filter design the user specifies the samples of the impulse response which reflects the desired filter properties. Speech synthesis as another application is widely encountered in telecommunications. In a communication channel the speech signals are carried as encoded waveforms. This helps to decrease the

size of the information that has been transferred. The receiver then decodes the incoming waveform and synthesizes the speech signal by generating the speech waveform according to the received filter coefficients. In text-to speech synthesis the system receiving the text, generates the corresponding speech signal combining the syllables that exist in the library. In time-frequency synthesis the user designs a signal that reflects the desired time-frequency properties.

Time-frequency analysis plays an important role in representing the frequency content of the signal as well as its energy spread. The time-frequency distributions that have been developed so far aim to show how the signal's energy has been distributed at which frequencies and when [1]. Therefore these distributions have an advantage over the Fourier analysis which only shows the frequency components of the signal and their relative strength. Wigner distribution is the first to be proposed and is the most widely used and studied. It has high resolution and high auto-term concentration [1, 2] but also contains cross terms which can interfere with the auto-components and decrease the interpretability of the Wigner distribution [3].

Time-frequency synthesis problem aims to design a signal that best reflects the desired time-frequency properties. These properties are summarized on a time-frequency model having a certain shape, and height on a two dimensional time-frequency plane. In the most general case, any two dimensional function may not correspond to the time-frequency distribution of any signal. The mapping is such that each signal has its time-frequency distribution but each model may not be the distribution of a signal, hence it is not invertible. Therefore in a typical synthesis problem, the cost between the model and the time-frequency distribution of the synthesized signal is aimed to be minimized.

Time-frequency signal synthesis is widely used for Ambiguity Function in Radar Signal Processing. Ambiguity Function is not an energetic time-frequency distribution but a correlative time-frequency representation. The user specified model contains the desired Ambiguity properties and by using Ambiguity based signal synthesis method, the signals with desired attributes are obtained.

The various applications related to time-frequency synthesis involve signal design [4], time frequency filtering [5], component extraction [4] and noise reduction [6]. In signal design the user constructs a model and aims to synthesize the signal whose time-frequency distribution is closest to that model. In time frequency filtering the user designs a filter that passes all the signals whose support lie in a time-frequency region and suppresses all the signals outside this region. First the time-frequency distribution such as Wigner distribution is computed. This is the analysis step. Then the signal's WD is multiplied by a mask which is the masking step and finally the output signal is synthesized from the masked WD which is the synthesis step. The mask is chosen such that it is one inside the pass region and zero outside [5]. Component Extraction is the time-frequency filtering for just single component. The user has the time domain representation of a multi-component signal and aims to separate one of its components. After computing the Wigner distribution of that multi-component signal masking is performed such that only the Wigner of the desired component is retained. This masked Wigner is then used as a model for the synthesis of the desired component [4]. Noise reduction is another application that is related to time-frequency synthesis. In general noise is typically spread throughout the time-frequency plane. If the noise is literally erased by masking and the signal support is retained then the resulting

time-frequency distribution will consist of only the signal and noise around that signal. The synthesized signal from that curtailed distribution will have considerably reduced noise. [6].

If signals with localized supports are aimed, then it is wise to use a Wigner distribution. Signal synthesis in Wigner domain concentrates on synthesizing a signal whose Wigner distribution is closest to a model Wigner. Model Wigner is a real-valued, square-integrable function of time and frequency. Various closeness measures can be adapted and least squares is the most commonly used.

The most primitive method is the Wigner distribution based synthesis algorithm [7, 8]. Second is the smoothed Wigner distribution-based synthesis algorithm which uses smoothed Wigner distribution where a signal whose smoothed Wigner is closest to the model is synthesized [4]. The third method is the masked Wigner distribution-based synthesis algorithm where a signal whose masked Wigner distribution is closest to the model is synthesized [9].

Various problems are encountered in signal synthesis in Wigner domain. First of all a Wigner distribution by its quadratic nature possess cross terms [10, 11]. There are two types of cross terms. Cross-cross terms emerge from the joint Wigner distribution [12] of two components whereas auto-cross terms emerge within the auto-Wigner of a single component. These cross terms are oscillatory and it is not easy to model them. In Wigner distribution-based signal design if the synthesis result is expected to have cross terms, the synthesis will not be satisfactory due to the difficulty in modeling these cross terms. In Wigner distribution-based component extraction, sometimes the cross-cross terms completely overlap a component that is to be extracted. In this case the

synthesis will not be successful because the component is buried under the cross terms coming from the other two components. As a solution to that problem it has been suggested to use smoothed Wigner distribution [4]. In this case the synthesis method aims to find a signal whose smoothed Wigner is closest to the time-frequency model. Smoothing corresponds to a two dimensional filtering of the Wigner distribution. This approach greatly reduces the drawbacks caused by cross terms but it is no more in Wigner domain. Another solution is the use of masked Wigner distribution which removes the need for the exact shape of the cross terms [9]. But here there is still need for the location of these terms.

Though the earlier approaches improve the drawbacks of the Wigner distribution-based signal synthesis, there still remain some problems. The smoothed and masked Wigner based synthesis methods proposed by [4, 9] are first of all computationally expensive. In the smoothing case, there is no optimum smoothing filter and no optimum smoothing parameters that will generate satisfactory results. In masked Wigner distribution-based synthesis, the specification of the don't-care mask, which is constructed according to the location of the cross terms may not be that easy especially in the signal design problem. Also if the the signal support is completely superimposed by the cross terms, the masked Wigner distribution-based synthesis will not produce the desired result.

The second common problem which is especially encountered in signal design is the specification of the model. When no time signal is available it is not easy to perfectly specify the model, especially the bandwidth distribution that will generate satisfactory results. Existing approaches did not directly propose a solution to this problem. It is generally left to the experience of the designer

who is expected to be familiar with the possible model shapes and bandwidth distributions. Actually the intuition about how the bandwidth distribution would be chosen is not something quite developed.

In this thesis, we focus on the signal design problem and propose a method that greatly facilitates the problems of earlier approaches. The main contribution of this thesis is to remove the need for cross term modeling because in transformed signal domain the cross terms are greatly reduced. Therefore the user does not have to worry about their shape and location. Also it facilitates the specification of the bandwidth which has a simpler shape in the transformed signal domain than in the original time domain. The proposed method is practical: the model parameters are easily specified. Finally it has a fast implementation.

The major steps of the novel design method are explained as follows: First of all, the user does not enter the model in the ordinary time-frequency plane but in the transformed signal domain. The parameters related to the model are progressively specified. First the spine which is the instantaneous frequency curve is determined in the ordinary time-frequency plane around which the signal energy would be distributed. Then, based on the orientation of the spine the rotation angle ϕ is computed such that the rotated spine is a single valued function of time. This rotation angle is used to determine the order of the fractional Fourier transformation [13, 14], which will be required in the last step of the design. Then the warping relations are computed which specify the center frequency for the model in warped domain [15]. After specifying the spine and the rotation angle in the original time domain, the bandwidth and amplitude distributions are specified in transformed signal domain. Model

Wigner is constructed using the parameters: bandwidth, amplitude and center frequency. After constructing the model a signal is synthesized in transformed signal domain using Wigner distribution-based synthesis algorithm. This algorithm is preferred because the interference terms are greatly reduced in the transformed signal domain. Then the synthesized signal is unwarped by a generalized unwarping relation which completes the design. The unwarping relation is the cascade of unwarping operation [15] and fractional Fourier transformation [13, 14]. Fractional Fourier transformation is used to rotate the signal's support in Wigner domain with respect to origin.

The organization of the thesis is as follows: First in Chapter 2 two of the existing design approaches are reviewed. They are the Wigner distribution based and the masked Wigner distribution based synthesis methods. Their theoretical formulation is presented and they are tested on simulation examples to discuss their performance. Then in Chapter 3 the novel design method is introduced. In this chapter, the fractional domain warping concept is explained, the method is presented and is tested on the cases where earlier approaches failed. Chapter 4 includes simulations for comparing the performances. It first deals with the synthesis of available time signals where the error between the original signal and designed signal is obtained for each method and compared. Then the synthesis of real signals is considered. Real signals are the recordings from nature such as birds, whales, etc. For real signals the performances are compared in terms of the fit to the desired region. Then the thesis is concluded.

Chapter 2

REVIEW OF EXISTING DESIGN APPROACHES

2.1 Wigner Distribution based Signal Synthesis

Signal synthesis problem is the design of a signal which exhibits some desired attributes. These attributes of the signal are usually specified in a convenient transform domain. Then a signal is generated such that it carries the desired attributes in the transform domain as much as possible. In time-frequency domain based signal synthesis problem, the desired attributes of the signal are specified in the time-frequency plane in the form of a model time-frequency distribution. The model time frequency distribution designates how the energy of the signal should be distributed as a joint function of both time and frequency.

In the classical approach, since the model may not be a valid time-frequency distribution, the signal is synthesized such that its computed time-frequency distribution is in some sense close to the model time-frequency distribution. Since the time-frequency distribution of a signal is not uniquely defined and the measure of closeness can be defined in a multitude of ways, the performance of the signal synthesis algorithm varies based on which closeness measure and time-frequency distribution definition are used.

One of the well known algorithms is the WD-based signal synthesis algorithm. Wigner Distribution is widely used if signals with localized supports are preferred. In this approach, the signal is designed such that its WD is the closest to the model time-frequency distribution in the least squares sense. For instance, when the model time-frequency distribution is denoted as $\mathcal{W}^M(t,f)$, the synthesized signal is generated as the solution to the following least squares minimization problem:

$$\begin{aligned} x_S(t) &= \arg\min_x J(x) && (2.1)\\ &= \arg\min_x \iint |\mathcal{W}^M(t,f) - W_x(t,f)|^2 \,\mathrm{d}t\,\mathrm{d}f \quad , && (2.2) \end{aligned}$$

where $x_S(t)$ is the synthesized signal, $J(x)$ is the cost function and $W_x(t,f)$ is the WD of the signal $x(t)$, which can be computed as

$$W_x(t,f) = \int x(t+t'/2)x^*(t-t'/2)e^{-j2\pi ft'}\,\mathrm{d}t' \quad . \tag{2.3}$$

In digital implementation, the continuous domain WD given in (2.3) is approximated by its discrete-time counter part $W_x[n,f)$ which is defined as

$$W_x(nT_s,f) \approx W_x[n,f) \triangleq T_s \sum_m c_x[n,m]e^{-j2\pi fmT_s} \quad , \tag{2.4}$$

where

$$c_x(n,m) = x[n+m]x^*[n-m] \tag{2.5}$$

is a correlation between the samples of the sequence $x[n]$ where $x[n] \triangleq x(nT_s)$ are the uniformly spaced samples of the continuous time signal $x(t)$ obtained with a sampling interval of T_s. Similarly the discretized model WD $\mathcal{W}^M[n,f) \triangleq \mathcal{W}^M(nT_s,f)$ can be expressed as:

$$\mathcal{W}^M[n,f) = T_s \sum_m c^{\mathcal{M}}[n,m] e^{-j2\pi f m T_s} \quad , \tag{2.6}$$

where $c^{\mathcal{M}}[n,m]$ is the inverse Fourier Transform of the model Wigner distribution

$$c^{\mathcal{M}}[n,m] = \int_{-1/2T_s}^{1/2T_s} \mathcal{W}^M[n,f) e^{j2\pi f m T_s} \, \mathrm{d}f \quad , \tag{2.7}$$

and in general it cannot be expressed as the outer product of a signal as in (2.5). Note that by discretizing the continuous time problem, we restrict the set of allowable signals in the optimization problem to those signals whose double-sided band-width B_x satisfies $B_x \leq 1/(2T_s)$.

After the discretization, the samples of the continuous time signal $x_S(t)$ are computed as a solution to the following minimization problem:

$$\begin{aligned} x_S[n] &= \arg\min_x J_D(x) && \text{(2.8a)} \\ &= \arg\min_x T_s^2 \sum_n \int_{-1/2T_s}^{1/2T_s} |\mathcal{W}^M(nT_s,f) - W_x(nT_s,f)|^2 \, \mathrm{d}f \quad , && \text{(2.8b)} \end{aligned}$$

where $x_S[n] = x_S(nT_s)$ and $J_D(x)$ denotes the discretized least squares cost function. As shown in Appendix A, by using the Parseval's relation the cost function $J_D(x)$ in (2.8) can be expressed as

$$J_D(x) = T_s \sum_n \sum_m |c_x[n,m] - c^{\mathcal{M}}[n,m]|^2 \quad , \tag{2.9}$$

where $c_x[n,m]$ and $c^{\mathcal{M}}[n,m]$ are given in (2.5) and (2.7). This result is similar to the one given in [9] where instead of $c^{\mathcal{M}}[n,m]$, $c^{\mathcal{D}}[n,m]$ is used corresponding

to the don't-care version. Since $x[n]$ is a half-band signal, its odd and even indexed samples are dependent. Thus, as shown in Appendix A, the above cost function can be expressed only in terms of the even indexed samples of the signal $x[n]$:

$$J_D(x) = T_s \left[\sum_n \sum_m |c^{\mathcal{M}}[n,m]|^2 + 2(\boldsymbol{x}_e^H \boldsymbol{x}_e)^2 - \boldsymbol{x}_e^H \tilde{\boldsymbol{D}}\, \boldsymbol{x}_e \right] \quad , \tag{2.10}$$

where the vector $\boldsymbol{x}_e$ consists of even indexed samples of the signal $x[n]$, and the entries of the matrix $\tilde{\boldsymbol{D}}$ are given in (A.22). The solution to this minimization problem is one of the stationary points of the cost function which is found by setting its complex gradient with respect to $\boldsymbol{x}_e^*$ to zero [16]:

$$\frac{\partial J_D(x)}{\partial \boldsymbol{x}_e^*} = T_s \left[4(\boldsymbol{x}_e^H \boldsymbol{x}_e) x_e - \tilde{\boldsymbol{D}}\, \boldsymbol{x}_e \right] = \boldsymbol{0} \quad , \tag{2.11}$$

which yields an eigenvalue problem

$$\tilde{\boldsymbol{D}}\, \boldsymbol{x}_e = 4\|\boldsymbol{x}_e\|^2 \boldsymbol{x}_e \quad , \tag{2.12}$$

where $\tilde{\boldsymbol{D}}$ is an Hermitian matrix. Thus if $(\lambda_i, \tilde{\boldsymbol{q}}_i)$ are ordered eigenpairs of the $\tilde{\boldsymbol{D}}$ matrix such that $\lambda_1 \geq \lambda_2 \geq \cdots$, then the stationary points of the cost function are in the form of

$$\boldsymbol{x}_{e,i} = \frac{\sqrt{\lambda_i}}{2} \tilde{\boldsymbol{q}}_i \quad . \tag{2.13}$$

By using Lemma 1, the even indexed samples of the synthesized signal are obtained as

$$\boldsymbol{x}_S = \frac{\sqrt{\lambda_1}}{2} \tilde{\boldsymbol{q}}_1 \quad , \tag{2.14}$$

where $\lambda_1 \geq \lambda_i$, $\forall i \neq 1$ and $\tilde{\boldsymbol{q}}_1$ is the corresponding eigenvector.

Lemma 1. *The global minimum of the cost function is obtained by choosing* $(\lambda_i, \tilde{\boldsymbol{q}}_i)$ *as the eigenpair with the maximum eigenvalue.*

Proof. Appendix B. □

Then by using the relation given in Appendix C, the odd indexed samples of the synthesized signal are recovered from the even indexed samples.

In the rest of this section, we investigate the performance of the WD based synthesis algorithm on simulated examples. In the first simulation, a model time-frequency distribution with a linear support is used. The model WD $W^{\mathcal{M}}(t, f)$ is chosen as the WD of a chirp signal as shown in Fig. 2.1 . In Fig. 2.2 (a), the result of the WD-based synthesis algorithm is given. To assess the performance of the algorithm, the WD of the synthesized signal is also computed as shown in Fig. 2.2 (b). By comparing the model WD given in Fig. 2.1 (b) and the WD of the synthesized signal Fig. 2.2 (b), we conclude that the WD based synthesis algorithm has a good performance for this simulation example.

Although the WD-based synthesis algorithm has produced very good results in this simulation, its success is very much dependent on the shape of the model WD. For instance, if the model WD has a linear time-frequency support as in this simulation, then this algorithm provides satisfactory results. However, if the model WD has a non-linear support in the time-frequency plane, then it would be difficult for the designer to incorporate the inner-interference term information into the model WD. Furthermore, if the model WD lacks the inner-interference term information [10, 11], this algorithm can provide very poor results.

In the second simulation, the synthesis of a non-linear chirp is considered. The synthetic signal shown in Fig. 2.3 (a) is used to generate the model WD.

This is achieved by removing the inner-interference terms of the WD of the chirp signal given in Fig. 2.3(b). The model WD obtained by this way contains only the auto-term structure as shown in Fig. 2.3(c). The WD-based synthesis algorithm on the model WD shown in Fig. 2.3(c) synthesized the signal shown in Fig. 2.4(a). By a close examination the WD of the synthesized signal given in Fig. 2.4 (b) and the model WD, it can be concluded that the synthesis algorithm performs poorly when the inner-interference terms are not included in the model WD.

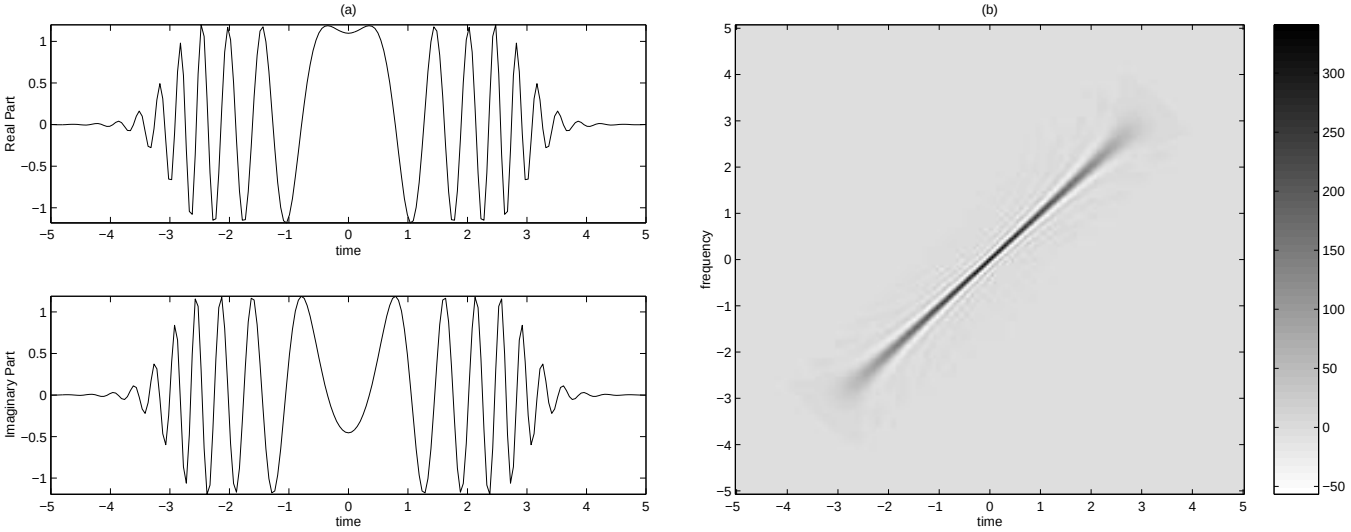

Figure 2.1: (a) The time domain representation of a chirp signal and (b) its Wigner distribution having a linear support. Interference terms are negligible.

2.2 Masked Wigner Distribution based Signal Synthesis Algorithm

To overcome the the difficulties associated with the WD-based synthesis algorithm in the cases where an accurate description of the inner-interference terms is not available, it has been suggested to use a masked Wigner distribution (MWD)-based signal synthesis algorithm [9]. In this approach, the design is performed by finding a signal whose *masked* WD is closest to the model WD in the least squares sense. In this approach the user creates a mask $M_{\mathcal{D}}(t, f)$ by designating the regions of time-frequency plane which covers the supports of the inner-interference terms. After specification of an appropriate don't-care

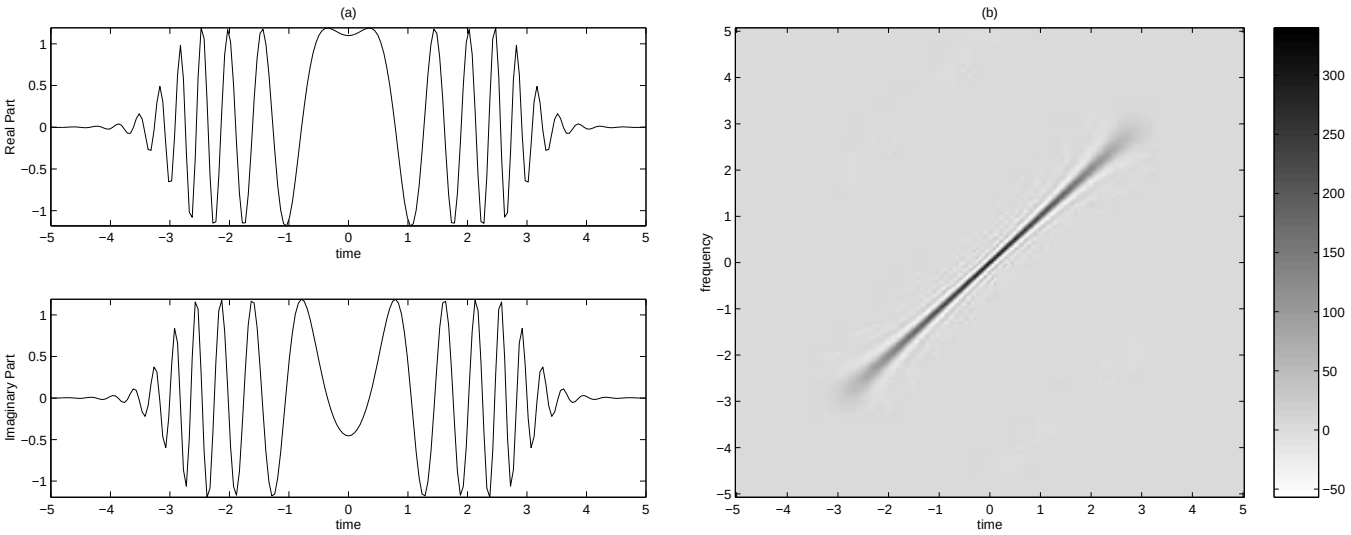

Figure 2.2: The simulation of the WD-based synthesis algorithm on the model time-frequency distribution given in Fig. 2.1(b): (a) The signal synthesized by using the WD-based synthesis algorithm and (b) the WD of the synthesized signal. The result is successful since the model did not require inner interference terms for a linear chirp signal.

mask as

$$M_{\mathcal{D}}(t,f) = \begin{cases} 1, & \text{if } (t,f) \notin \mathcal{D} \text{ i.e. the point } (t,f) \text{ is free-from cross term interference} \\ 0, & \text{if } (t,f) \in \mathcal{D} \text{ i.e. the point } (t,f) \text{ is contaminated with cross term interferenc} \end{cases} \tag{2.15}$$

where $\mathcal{D}$ denotes the *don't-care* region which covers the supports of the inner interference terms, the signal is synthesized as solution to the following minimization problem:

$$x_S(t) = \arg\min_x \iint [W^{\mathcal{M}}(t,f) - W_x^{(\mathcal{D})}(t,f)]^2 \,\mathrm{d}t\,\mathrm{d}f \quad , \tag{2.16}$$

where $W_x^{(\mathcal{D})}(t,f)$ is the masked Wigner distribution

$$W_x^{(\mathcal{D})}(t,f) \triangleq M_{\mathcal{D}}(t,f) W_x(t,f) \quad . \tag{2.17}$$

It should be noted that, MWD-based signal synthesis reduces to conventional WD-based signal synthesis method if the mask $M_{\mathcal{D}}(t,f)$ is chosen as unity at all points in the time-frequency plane.

To find the solution to the minimization problem given in (2.16), the gradient of the cost function is set to zero, and the obtained non-linear set of equations are solved. In [9], the iterative *quasi-power algorithm* is used to obtain a solution to these non-linear set of equations. The details of this algorithm and its fast implementation are discussed in [4, 9]. However it should be noted that its convergence rate is dependent on the shape of the don't-care mask and the appropriate initialization of the parameters and no formal proof of convergence of this algorithm is present so far.

Although, the MWD-based synthesis algorithm relieves the load of designer by requiring only the knowledge of the support of the cross-term interference but not its exact structure, its performance is very much sensitive to the shape of the *don't-care* mask. For instance if the designer is not an expert in this field or if the structure of the inner interference terms is too complicated, then he may not be able to accurately identify the support of the inner interference terms. He might either allocate too much or too little space for the don't care region. However, in this case spurious signal terms may appear in the synthesized signal, because in the cost function given in (2.16) the signal components inside $\mathcal{D}$ are not penalized as long as they do not lead to an interference term outside $\mathcal{D}$ [9]. For instance, if the model WD and the don't care masks are as shown in Fig. 2.5, then both of the signals given in Fig. 2.6 are solutions to the cost function of the MWD-based synthesis algorithm. To avoid this drawback of the algorithm, an energy penalty factor is incorporated into the definition of the cost function [9] which leads to a slight modification in the quasi-power algorithm. In general, the optimum choice of this parameter is not known, therefore it must be experimentally chosen. Choosing it too large results in

downscaling of the signal while choosing it too small results in incomplete suppression of the spurious signal components. [9]

2.2.1 Simulation of the MWD-based Signal Synthesis Algorithm

In this section, we investigate the performance of the MWD-based synthesis algorithm on the model WD which is given in Fig. 2.3 (c). A possible choice of the don't care mask is shown in Fig. 2.7 (a), where the don't care region is the dark colored region of the time-frequency plane. In this example, the energy penalty factor is chosen as zero. In all these simulation algorithms, the quasi power algorithm is initialized with a half-band white noise sequence. The synthesized signal and its Wigner distribution are shown in Fig. 2.7 (b) and Fig. 2.7 (c) respectively. By comparing the auto-term of the WD of the synthesized signal and the model WD given in Fig. 2.3 (c), it can be concluded that the MWD-based synthesis algorithm produced a very good result in this simulation.

In the second simulation the synthesis of a signal with a saw-toothed support is considered. In this case no time signal is available. The user designs the model Wigner and the don't-care mask. It's not easy to perfectly specify such a non-linear model because at the corners of the model the bandwidth is expected to become larger. But for the sake of simplicity a nearly constant bandwidth is chosen for the model Wigner given in Fig. 2.8 (a). The idea behind choosing this example is that the middle portion of the Wigner support would be superimposed by the inner-interference terms caused by the tails.

To speak more clearly, the first and third up-ramping parts would cluster the second up-ramping portion, similarly the first and third down-ramping parts would cluster the second down-ramping portion. Therefore the middle part of the model support should be included inside the don't-care region which is shown in Fig. 2.8 (b). Black areas correspond to cross term interference. The synthesis results are depicted in Fig. 2.9 (a),(c),(e),(g) for energy penalty factors of $\gamma = 0,\ 0.05,\ 0.1,\ 0.15$. From the Wigner distribution plots given in Fig. 2.9(b),(d),(f),(h) it can be concluded that the MWD-based synthesis algorithm cannot successfully recover the middle portion of the model. This is the result of including this region in the definition of the don't-care mask because of the overlap between the cross-terms with the auto-term at that region.

In the third case, the model is obtained from a time signal given in Fig. 2.10(a). The Wigner distribution is shown in Fig. 2.10(b). In this simulation, the aim is to supply a model which is obtained from a Wigner distribution and is free from interference terms. It should be noted that no smoothing is performed. The model Wigner is obtained by multiplying the Wigner with the don't-care given in Fig. 2.10(d). The don't-care mask is obtained using the interference term information in Fig. 2.10(b). The synthesis results are depicted in Fig. 2.11 (a),(c),(e),(g) for energy penalty factors of $\gamma = 0,\ 0.05,\ 0.1,\ 0.15$. From the Wigner distribution plots given in Fig. 2.11 (b),(d),(f),(h) it can be concluded that the MWD-based synthesis algorithm cannot successfully recover the middle portion of the model even if the model is obtained from a Wigner distribution and a nearly perfect don't-care mask is used.

In the fourth simulation, the model is chosen as the Wigner of the signal shown in Fig. 2.12 (a). The don't care mask is again obtained using the interference term information. The synthesis results are depicted in Fig. 2.13 (a),(c),(e),(g) for energy penalty factors of $\gamma = 0,\ 0.05,\ 0.1,\ 0.15$. From the Wigner distribution plots given in Fig. 2.13 (b),(d),(f),(h) it can be concluded that the MWD-based synthesis algorithm again cannot successfully recover the middle portion of the model. This time all the input parameters were ideal: the model exactly same as the Wigner, don't-care perfectly localizing the inner-interference term support, etc. In the last two simulations there existed spurious signal components in the synthesis results when low energy penalty factors are used. This is because of the fact that there is auto-term support inside don't-care mask and there is no information outside the don't-care mask that will contribute for the synthesis of these auto-terms. Therefore it becomes necessary to increment the energy penalty which results in down-scaling of the auto-terms.

From all these simulations it can be concluded that the performance of the MWD-based synthesis algorithm is directly affected by the interference term support which determines the shape of the don't care region. If the interference terms superimpose any auto-term support, then that part of the signal may not be recovered. Also it is not easy to correctly specify the model at the beginning if no time signal is available and choosing a model far from the possible synthesis result may lead to unacceptable designs.

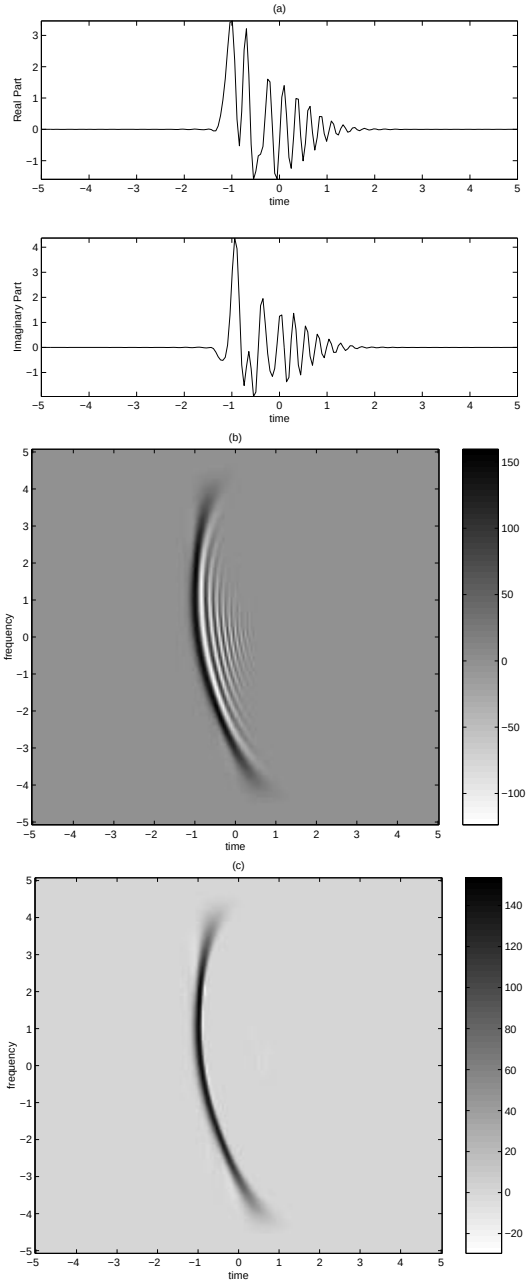

Figure 2.3: (a) The time domain representation of a non-linear chirp signal, (b) its Wigner distribution and (c) the model Wigner distribution which is obtained by removing the inner-interference terms of the WD given in (b). In the most general case the time domain representation will not be available and the model will not contain interference terms due to apparent difficulty in modeling such terms.

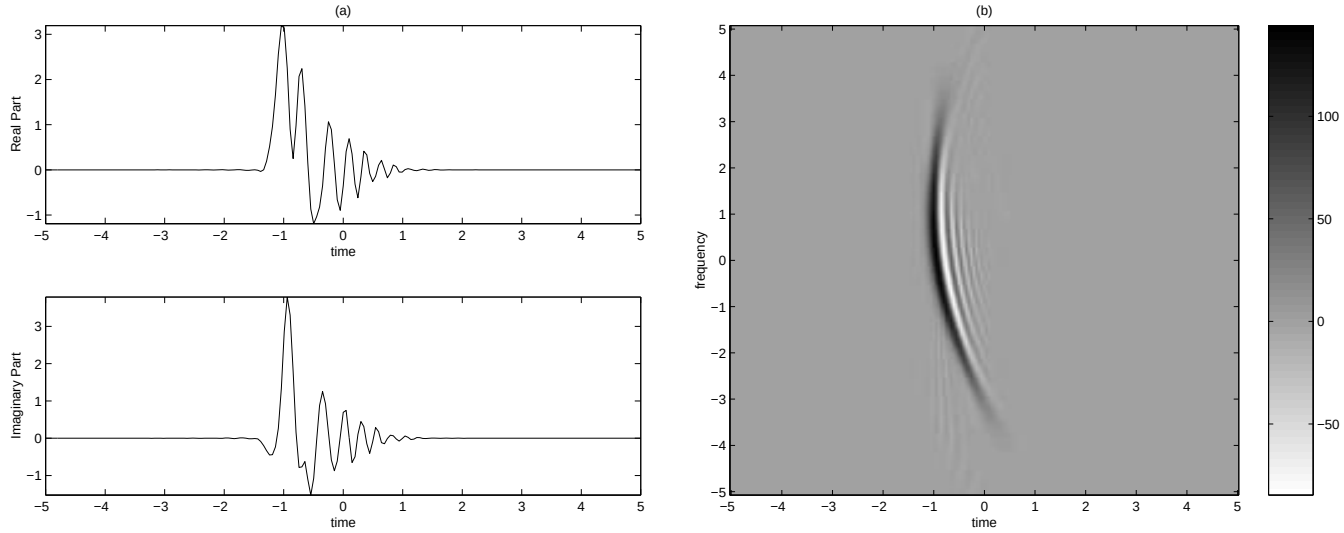

Figure 2.4: The simulation of the WD-based synthesis algorithm on the model time-frequency distribution given in Fig. 2.3 (b): (a) The signal synthesized by using the WD-based synthesis algorithm and (b) the Wigner distribution of the synthesized signal. The resulting synthesized signal cannot fit completely to the desired region because the model lacked inner interference terms. The performance therefore, though not very poor, is not satisfactory even if the inner interference terms are likely to occupy a small region.

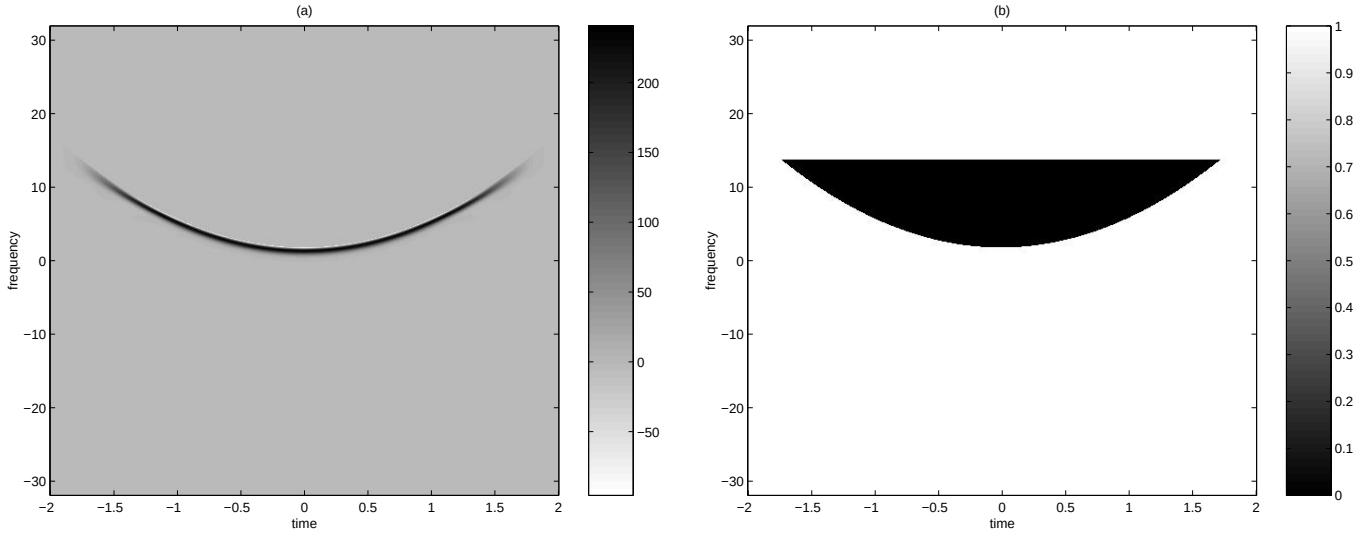

Figure 2.5: (a)The model time-frequency distribution, (b) the don't-care region used for the MWD-based synthesis algorithm. It is guessed so that it is compact enough and safely covers the expected interference terms.

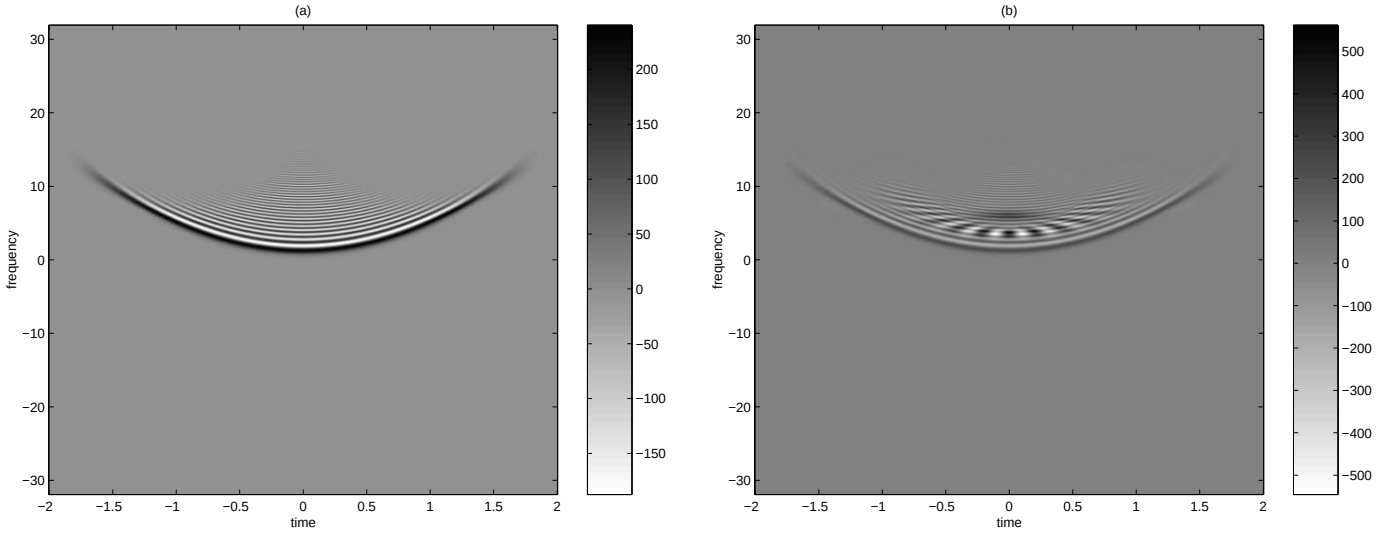

Figure 2.6: (a) A Solution for the MWD-based synthesis algorithm consisting of a quadratic chirp, and (b) another solution with the same cost as (a) consisting of a quadratic chirp and a gaussian which is submerged in interference term support of the quadratic chirp.

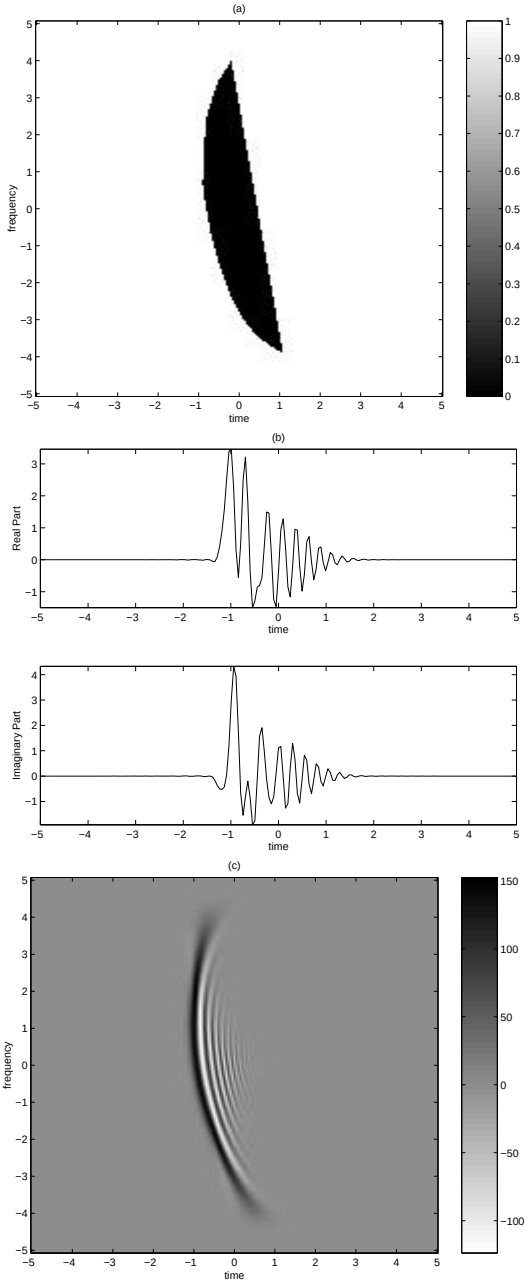

Figure 2.7: The simulation of the MWD-based synthesis algorithm on the model time-frequency distribution given in Fig. 2.3 (b): (a) The don't care mask $M(t, f)$, (b) the signal synthesized by using the MWD-based synthesis algorithm and (c) the Wigner distribution of the synthesized signal. The synthesis result is quite satisfactory. Therefore MWD-based synthesis algorithm does not require the modeling of the inner interference terms but guessing their location.

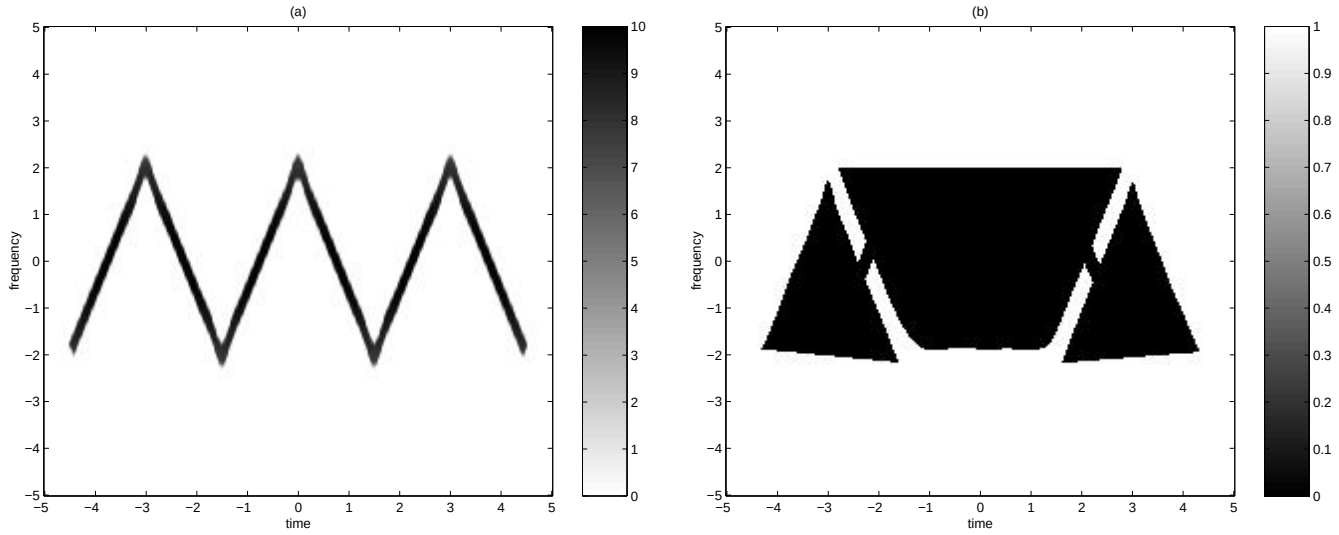

Figure 2.8: (a) The model Wigner, (b) Don't-care Mask $M(t, f)$. In model, the first and third up-ramping parts would cluster the second up-ramping portion, similarly the first and third down-ramping parts would cluster the second down-ramping portion. Also the first and second up-ramping parts would cluster the first down-ramping component, similarly the second and third down-ramping portions would cluster the third up-ramping portion. Therefore the don't-care mask is chosen as shown in (b).

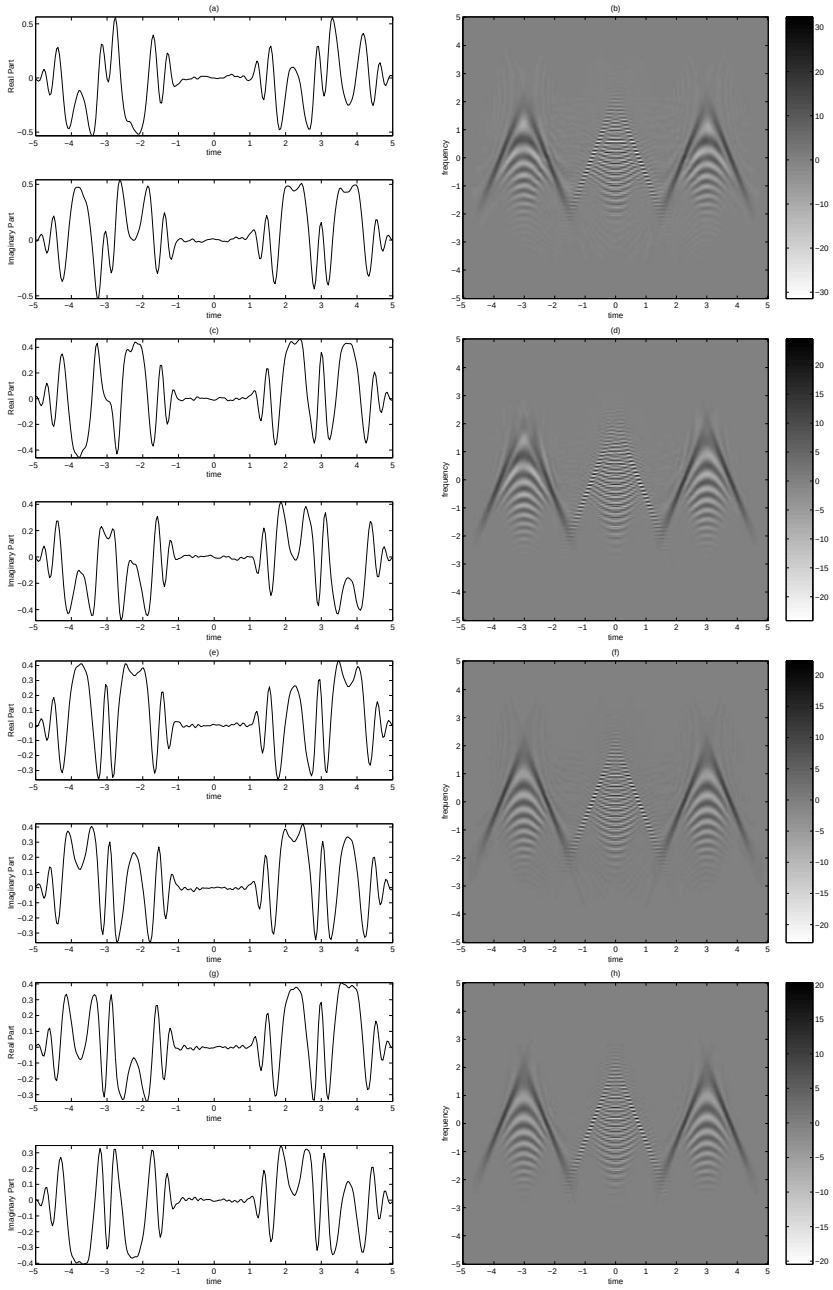

Figure 2.9: The simulation of the MWD-based synthesis algorithm on the model time-frequency distribution given in Fig. 2.8 (a): On the left the signals synthesized by using the MWD-based synthesis algorithm with penalty factors of (a) 0, (c) 0.05, (e) 0.1 and (g) 0.15 are shown. In (b), (d), (f) and (h) the WD of each synthesized signal is given next to the corresponding signal. The results are not satisfactory for different values of energy penalty factors because of the fact that don't-care mask covered the middle portion of the component and the algorithm perceived the situation as the synthesis of two separate components.

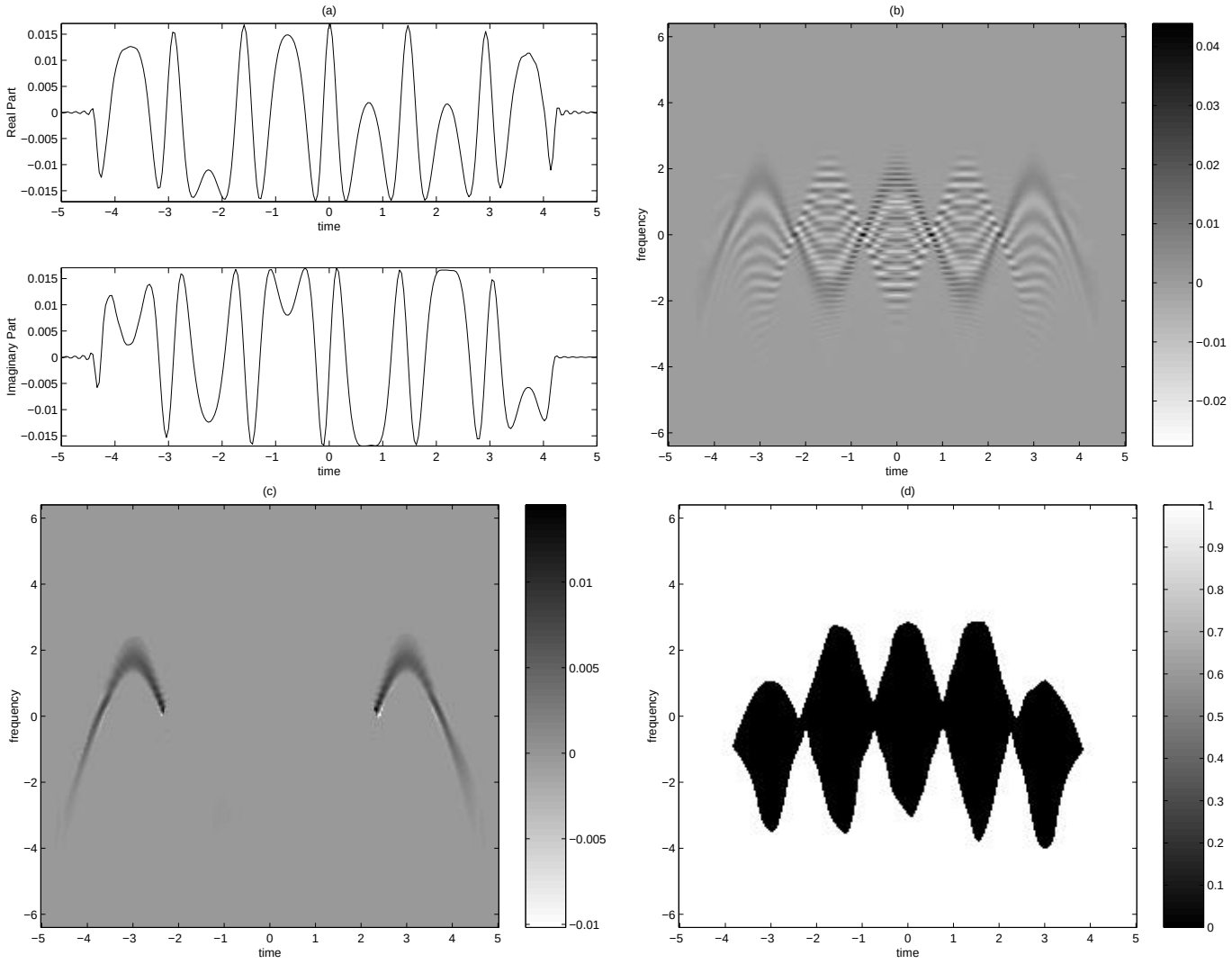

Figure 2.10: (a) The time domain representation, (b) its Wigner distribution, (c) Model WD obtained by multiplying the Wigner in (b) with don't-care in (d), (d) Don't-care Mask $M(t, f)$. The cross term free model is obtained from a Wigner distribution of a signal. Wigner is multiplied with don't-care mask which is obtained using the interference term support of the available time domain representation.

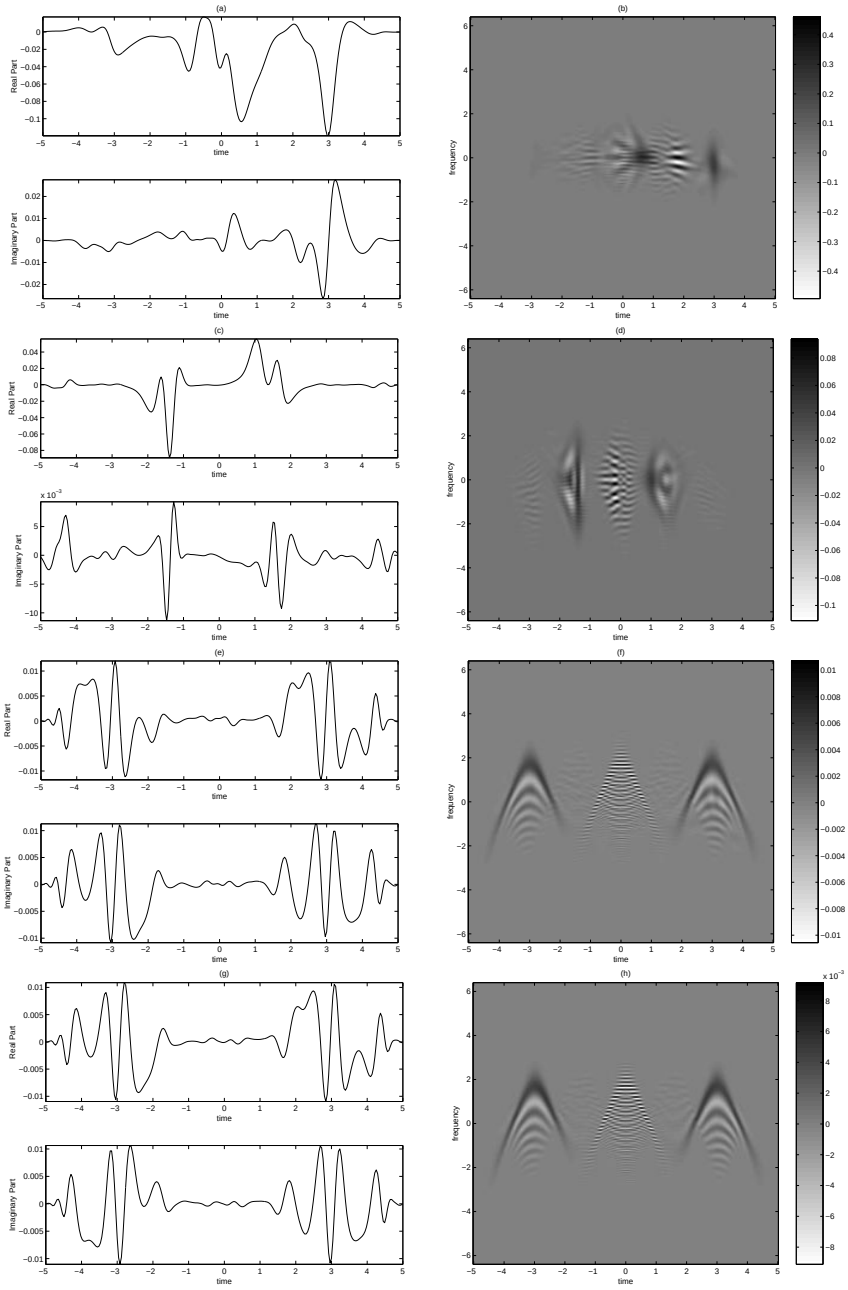

Figure 2.11: The simulation of the MWD-based synthesis algorithm on the model time-frequency distribution given in Fig. 2.10(c): On the left the signals synthesized by using the MWD-based synthesis algorithm with penalty factors of (a) 0, (c) 0.05, (e) 0.1 and (g) 0.15 are shown. In (b), (d), (f) and (h) the WD of each synthesized signal is given next to the corresponding signal. The synthesis results for various penalty factors are unsuccessful even if the correct don't-care mask is entered. The middle portion could not be synthesized due to clustering of inner interference terms.

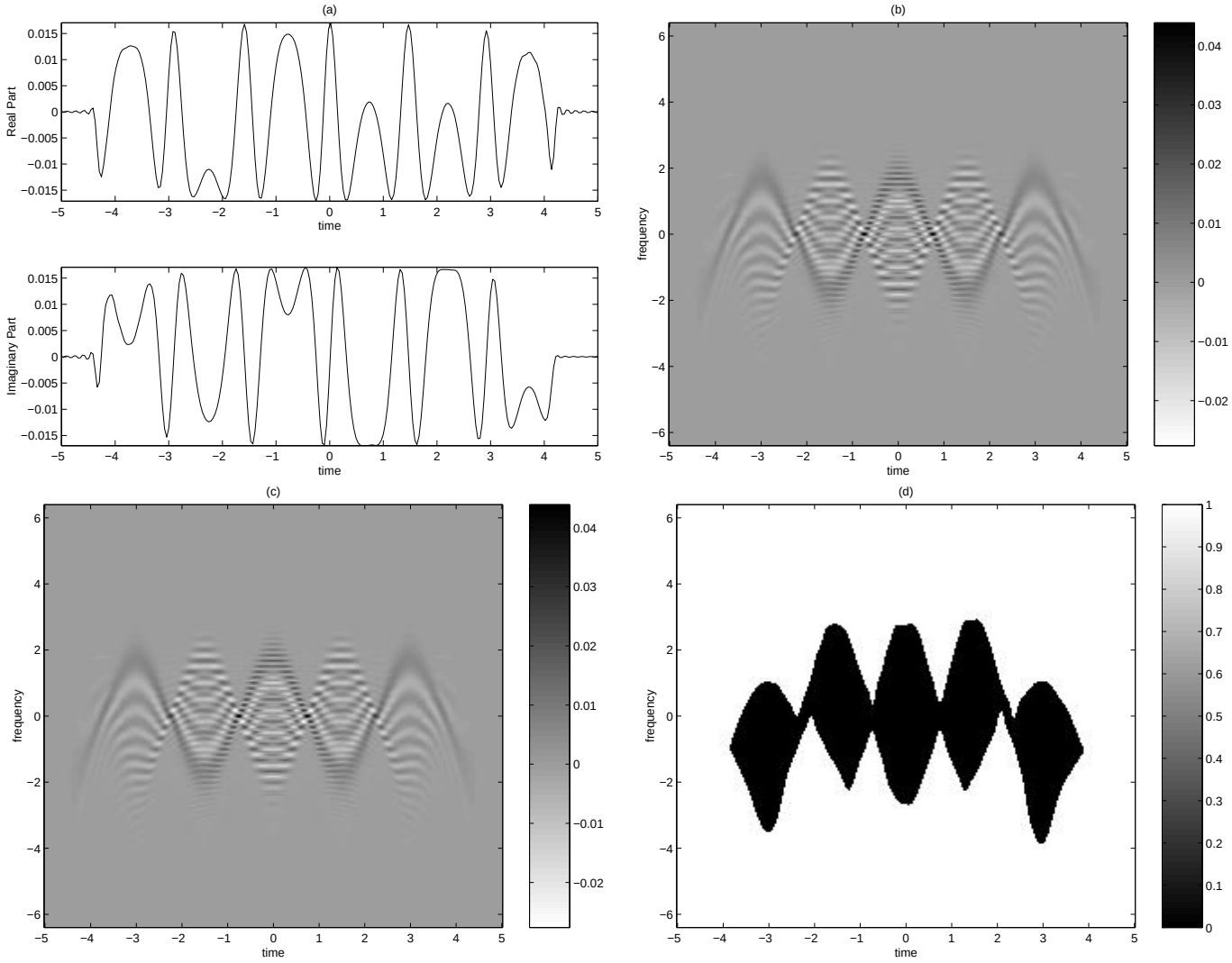

Figure 2.12: (a) The time domain representation, (b) its Wigner distribution, (c) Model WD same as the Wigner in (b), (d) Don't-care Mask $M(t, f)$. In this case, the model is chosen as the Wigner of the time signal which includes all the necessary information about the signal. The don't-care mask is chosen again using the inner interference term spread of the time signal.

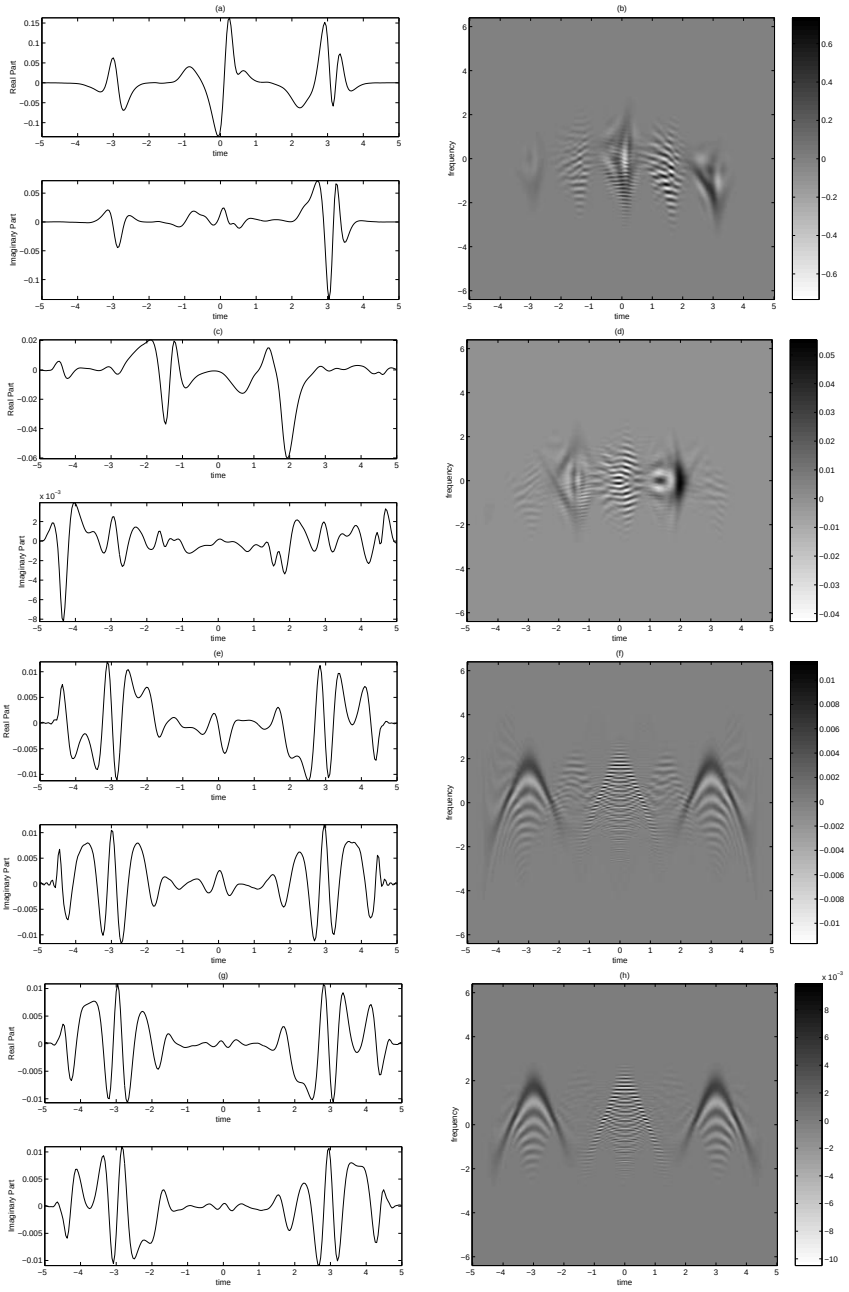

Figure 2.13: The simulation of the MWD-based synthesis algorithm on the model time-frequency distribution given in Fig. 2.12(c): On the left the signals synthesized by using the MWD-based synthesis algorithm with penalty factors of (a) 0, (c) 0.05, (e) 0.1 and (g) 0.15 are shown. In (b), (d), (f) and (h) the WD of each synthesized signal is given next to the corresponding signal. The results for various energy penalty factors are unsuccessful because of the same reason: The middle portion is completely clustered by inner interference terms.

Chapter 3

A Novel Wigner Distribution based Design Method using Fractional Domain Warping

In this section, we present a novel signal design approach which avoids the drawbacks of the algorithms discussed in the previous sections and at the same time simplifies the solution of the design problem. The basic problems with the existing approaches are caused by the inner interference terms and model specification.

The difficulty inner interference terms create deeply affects the performance of the synthesis results. Such terms are not easy to model. It is difficult to predict their exact location and shape if no time signal is available. Therefore supplying a cross term free model to WD-based synthesis algorithm, the result will be poor. MWD-based algorithm avoids the necessity for the exact shape

of interference terms. The exact location is still not known but can be guessed in determining the don't-care mask. But even in this case if the cross terms are likely to overlap some of the auto-term support such parts can be lost in the design.

On the other hand the inaccuracy in determining a reasonable model affects the overall performance. The most significant parameter in model selection is the bandwidth. There is no common agreement on how the bandwidth should be selected. It is not constant throughout the signal's support. Observations show that it enlarges at the corners and end points. How much should this enlargement be is a matter of obscurity.

We facilitate the two problems addressed so far. The model is easily specified and with the aid of transformed signal domains, the need for auto-cross terms is greatly reduced. The design is complete when the synthesized signal in transformed signal domain is unwarped back to the ordinary time domain.

3.1 Specification of the Model

In the new method, instead of directly constructing a 3-D model time-frequency distribution and synthesizing a signal based on this model, the user specifies the parameters of the model progressively. The user first specifies the *spine* of the signal. We use the term spine interchangeably with the instantaneous frequency information. It is the curve in time-frequency plane around which the signal energy is spread. Spine can be any shape as long as a Wigner distribution can be built onto it. For the specification of the spine, the user either describes it by an analytical expression, or marks a finite number of points which reside

on the spine and then connects these points by using interpolation such as the spline interpolation algorithm. As an example a Wigner Distribution overlayed with the spine is shown in Fig. 3.6 (c). Here a representative number of points on the spine are highlighted.

The second parameter is the bandwidth distribution around the spine. Instead of determining the bandwidth in the ordinary time-frequency plane, we propose to specify it in the transformed signal domain where it is much more simple. Possible choices for the bandwidth can be a constant, a shifted gaussian, inverted and shifted gaussian and similar curves. These are illustrated in Fig. 3.2 (d).

The relation between the transformed signal domain and the ordinary time domain is explained in the next section.

3.2 Fractional Domain Warping

The new algorithm is based on the fractional domain warping concept, which was first introduced in [15]. In this approach, the design problem is transformed into a new domain where no interference terms exist. Thus, the most important advantage of the new approach is that, it is not necessary to know the structure and location of the inner interference terms. Therefore, there is no need to construct a don't-care mask which can be burdensome for complicated interference term structures. Furthermore, it is very practical since the user can easily choose the appropriate design parameters. And finally it offers a very efficient implementation. Before presenting the full details of the new

algorithm, we briefly discuss one of its key components: the fractional domain warping.

Time domain warping corresponds replacing the time dependence of a signal with a warping function. If $x(t)$ is the signal to be warped, and $\zeta(t)$ is the warping function then the warped signal is given as $x_\zeta(t) = x(\zeta(t))$. For the invertibility of the warping operation, $\zeta(t)$ should be chosen as a one-to-one and differentiable function. Typically, time domain warping is used in processing of the frequency modulated (FM) signals. As an example let $x(t)$ be $A(t)e^{j2\pi\phi(t)}$, where $A(t)$ is the non-negative amplitude and $\phi(t)$ is the phase. In this case when the warping function is chosen as $\zeta(t) = \phi^{-1}(f_s t)$ where $f_s > 0$ is an arbitrary scaling constant, the warped signal becomes

$$x_\zeta(t) = A(\zeta(t))e^{j2\pi f_s t} \quad , \tag{3.1}$$

which is a sinusoidal function at f_s with envelope $A(\zeta(t))$. In general it would be easier to operate on this function and if the warping relation is one-to-one, then the original signal can be recovered by the following unwarping operation

$$x(t) = x_\zeta(\zeta^{-1}(t)) \quad . \tag{3.2}$$

In our application, the warping function will be computed from the *spine*, $\psi(t)$, of the signal around which the signal energy is localized. When the spine is single valued it is also called the instantaneous frequency. The spine of the signal can be obtained either automatically by using a slightly modified instantaneous frequency estimation algorithm or manually by marking several points $(t_i, \psi(t_i))$ of the spine on the time-frequency plane and then connecting them by using an interpolation algorithm such as the spline interpolator [17]. After estimating the spine of the signal, for a signal with time domain support

$t_1 \leq t \leq t_N$, the warping function and its inverse are computed as

$$\Gamma(t) = \int_{t_1}^{t} \psi(t')\,\mathrm{d}t' \quad , \quad t_1 \leq t \leq t_N \tag{3.3}$$

$$\zeta^{-1}(t) = \Gamma(t)/f_\psi + t_1 \quad , \quad t_1 \leq t \leq t_N \tag{3.4}$$

$$\zeta(t) = \Gamma^{-1}(f_\psi(t - t_1)) \quad , \quad t_1 \leq t \leq t_N \quad , \tag{3.5}$$

where f_ψ is the mean of the spine

$$f_\psi = \Gamma(t_N)/(t_N - t_1) \quad . \tag{3.6}$$

For the invertibility of the warping operation, the $\Gamma(t)$ function given in (3.3) should be one-to-one which is ensured only when the $\psi(t)$ is a strictly positive function of time. If this condition is not satisfied, then warping operation can be performed on the frequency modulated version of the signal. In this case, the new spine would be a frequency shifted version of the former one.

This warping operation has the effect of transforming a signal with a curved time-frequency support to a signal with a linear time-frequency support which is concentrated around the center frequency, f_ψ. Thus, after the warping operation the inner interference terms of the signal are considerably reduced. Therefore the designer does not have to worry about the structure or location of the inner interference terms which was a hurdle in the conventional signal design process. After unwarping the signal designed in the warped domain, complicated signals with non-linear supports can be designed. However the time domain warping technique fails if the spine is not a single valued function of time as in Fig. 3.1 (b). To utilize the warping concept for this type of spines which can be converted into a single valued function of time after a rotation in time-frequency plane, the time domain warping is extended to fractional Fourier domains [18].

In fractional domain warping, instead of the time signal $x(t)$ its fractional Fourier transform (FrFT) which is defined as [13, 14, 19] is warped.

$$x_a(t) \equiv \{\mathcal{F}^a\, x\}(t) \triangleq \int K_a(t,t')x(t')\,\mathrm{d}t' \quad , \tag{3.7}$$

where $a \in \Re$ is the order of the transformation and $K_a(t,t')$ is the kernel of the transformation given in [14]. A number of interesting properties of FrFT can be found in [14]. In this paper, we make use of the rotation property of the FrFT, which states that the WD of the a^{th} order FrFT of a signal is the same as the WD of the original signal rotated by an angle of $a\pi/2$ radians in the clock–wise direction [14]. For instance in Fig. 3.1 (b) and Fig. 3.1 (d), the WDs and spines of the signal $x(t)$ and its FrFT $x_a(t)$, $a = -0.909$, are shown. The importance of these figures in terms of warping is the following: Although time–domain warping is not useful for the processing of $x(t)$, since this signal does not have a singled–valued instantaneous frequency, it is perfectly well suited to its a^{th} order FrFT. Therefore the fractional domain warping extends the class of signals for which warping concept is applicable.

When the time domain signal is available, the algorithm given in Algorithm 1 can be used for warping and unwarping of the signal. The warping part of this algorithm is illustrated in Fig. 3.1. The use of the fractional domain warping concept in the signal design problem where the time domain signal is not available, will be discussed in the next section.

Algorithm 1 The Fractional Domain Warping Algorithm

Steps of the Warping Part of the Algorithm:

1. Identify the support of the signal component in the time-frequency plane.
2. Based on the orientation of the signal component, determine the fractional Fourier transform order a.
3. Compute the a^{th} order FrFT $x_a(t)$ of the signal.
4. Estimate the spine $\psi(t)$ of the signal $x_a(t)$ by using the spline interpolation.
5. If the spine takes negative values, frequency modulate the input signal by Δ_f so that the shifted spine $\psi_{\Delta_f}(t) \triangleq \psi(t) + \Delta_f$ is strictly positive.
6. Compute the warped signal $x_{a,\Delta_f,\zeta}(t) \triangleq x_{a,\Delta_f}(\zeta(t))$ by warping the frequency modulated signal $x_{a,\Delta_f}(t) = x_a(t)e^{j2\pi\Delta_f t}$ using the spine $\psi_{\Delta_f}(t)$ according to the warping relation given in (3.3).

Steps of the Unwarping Part of the Algorithm:

7. After processing the warped signal $x_{a,\Delta_f,\zeta}(t)$ by some operator $\aleph(\cdot)$, its output $y_{a,\Delta_f,\zeta}(t) \triangleq \aleph(x_{a,\Delta_f,\zeta}(t))$ is unwarped and demodulated: $y_a(t) = e^{-j2\pi\Delta_f t} y_{a,\Delta_f,\zeta}(\zeta^{-1}(t))$
8. Finally the time domain representation of the output signal is computed by using the inverse fractional Fourier transform: $y(t) \equiv \{\mathcal{F}^{-a}\, y_a\}(t)$.

3.3 Signal Design Using Fractional Domain Warping

As discussed in the previous sections, the difficulty in modeling the inner interference terms complicates the signal design problem. Since in the new method, the signal will be synthesized in warped domain, the signal model will be free from cross-term interference. Therefore, the WD-based synthesis algorithm can be used to obtain the designed signal in the warped domain. Then, by unwarping this signal, the time domain representation of the designed signal is obtained. For the sake of clarity, the steps of the algorithm will be illustrated on an example.

In the new method, the user specifies the parameters of the model progressively. For instance, in this example the user first specifies the spine of the

signal as shown in Fig. 3.2 (a). Then, based on the orientation of the spine the rotation angle ϕ is computed. The rotation angle is chosen such that, after rotation of the spine by ϕ radians in the clockwise direction, the rotated spine $\psi(t)$ becomes a single valued function of time as shown in Fig. 3.2 (b). The significance of rotation is that, it corresponds to the design of the signal in $(2\phi/\pi)^{\text{th}}$ fractional Fourier transform domain. Therefore in the last step, the $(-2\phi/\pi)^{\text{th}}$ order fractional Fourier transform of the designed signal based on the rotated spine should be computed to obtain the time domain representation of the synthesized signal.

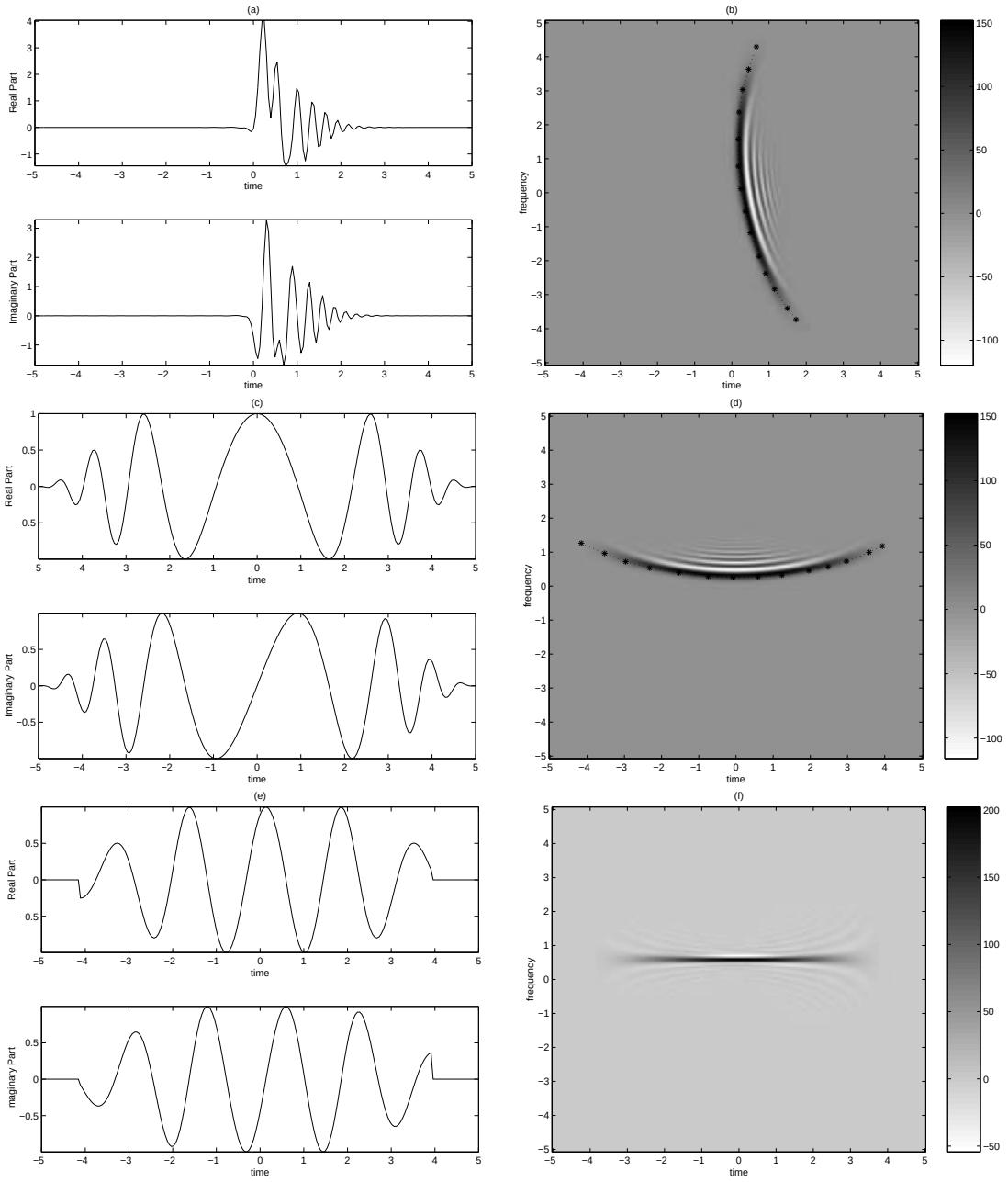

Figure 3.1: (a) The time domain representation of the signal $x(t)$, (b) its Wigner distribution $W_x(t, f)$ overlaid with the spine, (c) the $a = -0.909^{\text{th}}$ order FrFT $x_a(t)$ of the signal $x(t)$, (d) the WD $W_{x_a}(t, f)$ of $x_a(t)$ overlaid with the spine (e) the time domain representation of the warped signal and (f) its Wigner distribution. Note that warped signal has a horizontal support free from cross terms.

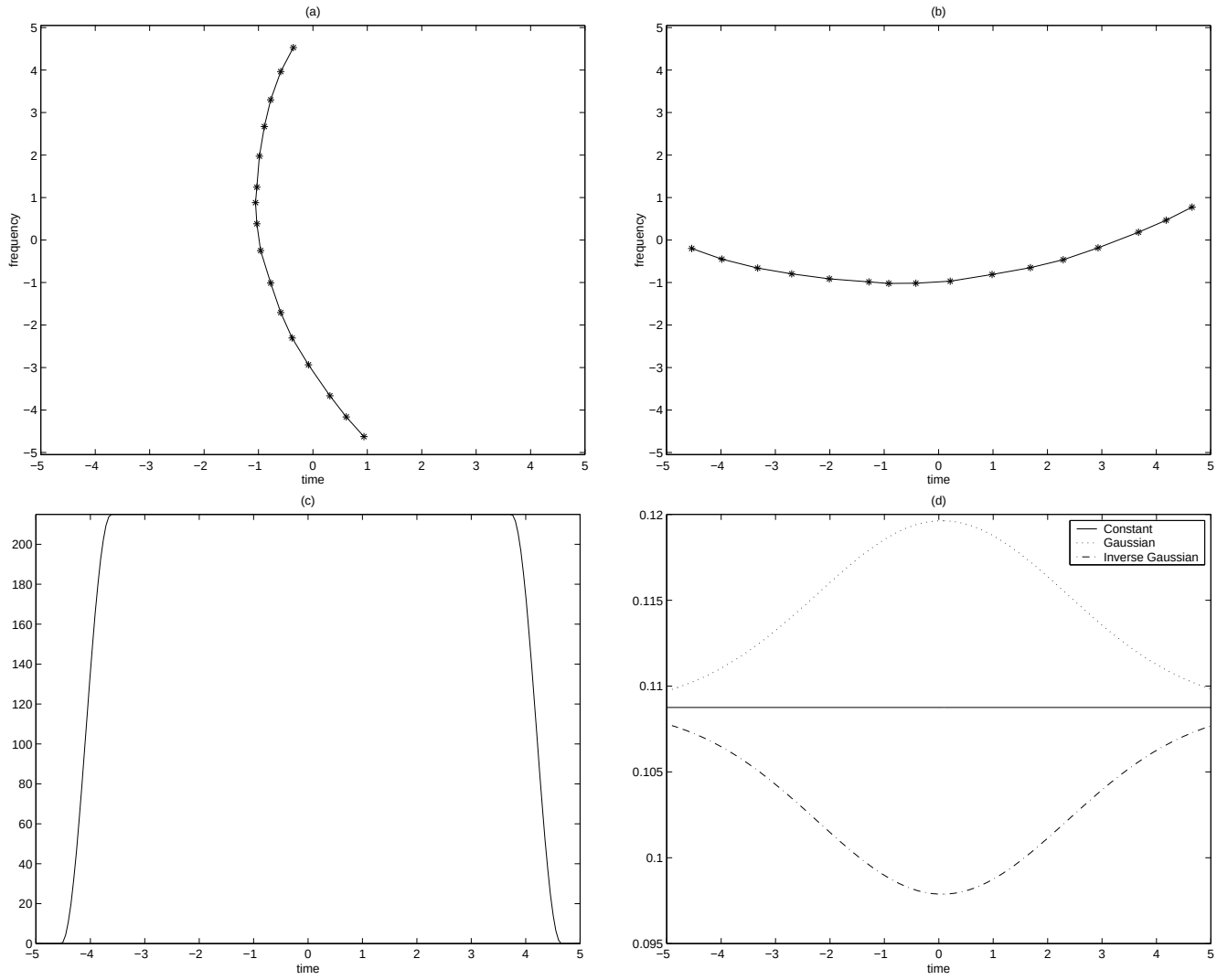

Figure 3.2: The parameters specified by the designer: (a) spine, (b) its rotated form $\psi(t, f)$, (c) the envelope $m(t)$ and (d) the instantaneous bandwidth $B_i(t)$. (a) and (b) is specified in original time domain, (c) and (d) are specified in transformed signal domain.

After the rotation of the spine, the warping function $\zeta(t)$, inverse of the warping function $\zeta^{-1}(t)$ and the center frequency f_ψ of the rotated spine are computed by using (3.3)-(3.6). Note that for the invertibility of the warping function, in the rotated time-frequency plane, the spine curve should be a strictly positive function of time as discussed in Section 3.2. If this condition is

not satisfied, then the spine is translated along the frequency direction by an appropriate amount to make it strictly positive. Then, the signal designed in the fractional Fourier transform domain should be demodulated by the same amount to remove the effect of frequency-translation of the spine.

After specification of some of the signal parameters related to the warping function in the usual time-frequency domain, the other parameters are specified in the *warped* time-frequency domain. One of these parameters is the envelope $m(t)$ of the warped time-frequency representation which is chosen only as a function of time for simplicity. The envelope can be chosen from a large variety of selections. In this example, it is chosen as a raised cosine pulse as shown Fig. 3.2 (c). Finally, the designer specifies the double-sided instantaneous bandwidth $B_i(t)$ of the model in the warped time-frequency domain. In this example, the instantaneous bandwidth is chosen as a raised and inverted Gaussian pulse as shown in Fig. 3.2 (d). Based on these 1-D parameters, the 3-D model time-frequency distribution $\tilde{W}(t,f)$ is constructed as

$$\tilde{W}(t,f) = \exp\left\{\frac{(f-f_\psi)^2}{2\sigma^2(t)}\right\} m(t) \quad , \tag{3.8}$$

where $\sigma(t) = B(t)/4$. In other words, at each time instant the model time frequency representation is a Gaussian signal with a double-sided bandwidth $4\sigma(t)$ as a function of frequency. The model time-frequency distribution constructed by this equation is shown in Fig. 3.3.

Since, in the warped domain, the constructed signal model has a linear support in the time-frequency domain, the designer can choose any of the synthesis algorithms which produces good results for this class of signals. In this method, we propose to use the WD-based synthesis algorithm for this purpose, because this algorithm has a good performance for this type of model

time-frequency distributions. Furthermore this algorithm is not iterative like the MWD-based algorithms as discussed in Section 2.2. Therefore it is faster and it does not have a convergence problem. In this simulation by using the WD-based synthesis algorithm on the model WD given in Fig. 3.3 the signal shown in Fig. 3.4 (a) is synthesized in the warped fractional Fourier domain. The WD of this signal is plotted in Fig. 3.4 (b). Then by unwarping this signal the $(-0.909)^{\text{th}}$ order FrFT of the synthesized signal is obtained as shown in Fig. 3.5 (a). The WD of this signal is given in Fig. 3.5 (b). Finally by computing the 0.909 ordered FrFT, the time domain representation of the synthesized signal and its Wigner distribution are obtained as shown in Fig. 3.6 (a) and Fig. 3.6 (b), respectively. As shown Fig. 3.6 (c), the spine of the designed signal is the same as the user specified spine shown in Fig. 3.2 (a).

For the sake of comparison, the proposed synthesis method is used to design the signals which are tough cases for the WD and MWD-based synthesis algorithms. The case where WD-based algorithm failed is already examined, the result of which is given in Fig. 3.6. The result of the proposed synthesis method in the case where MWD-based synthesis algorithm failed is given in Fig. 3.7 and Fig. 3.8 . Thus by comparing the obtained results of all the algorithms, the superior performance of the novel algorithm can easily be appreciated.

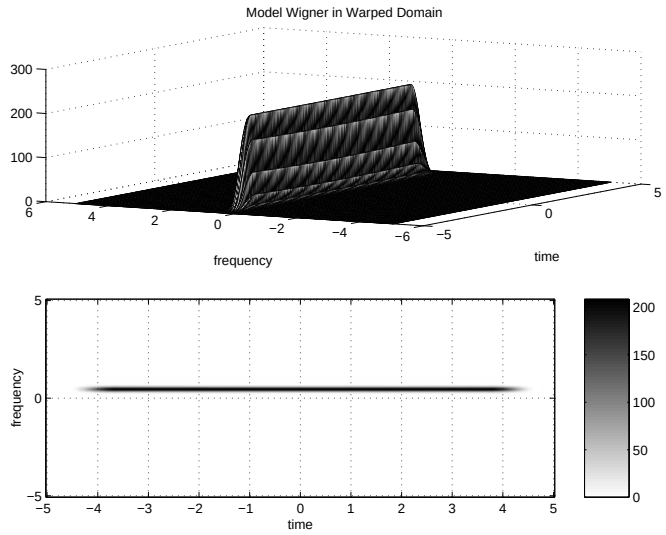

Figure 3.3: The model time-frequency distribution in the rotated and warped time-frequency plane, which is computed by using the parameters given in Fig. 3.2.

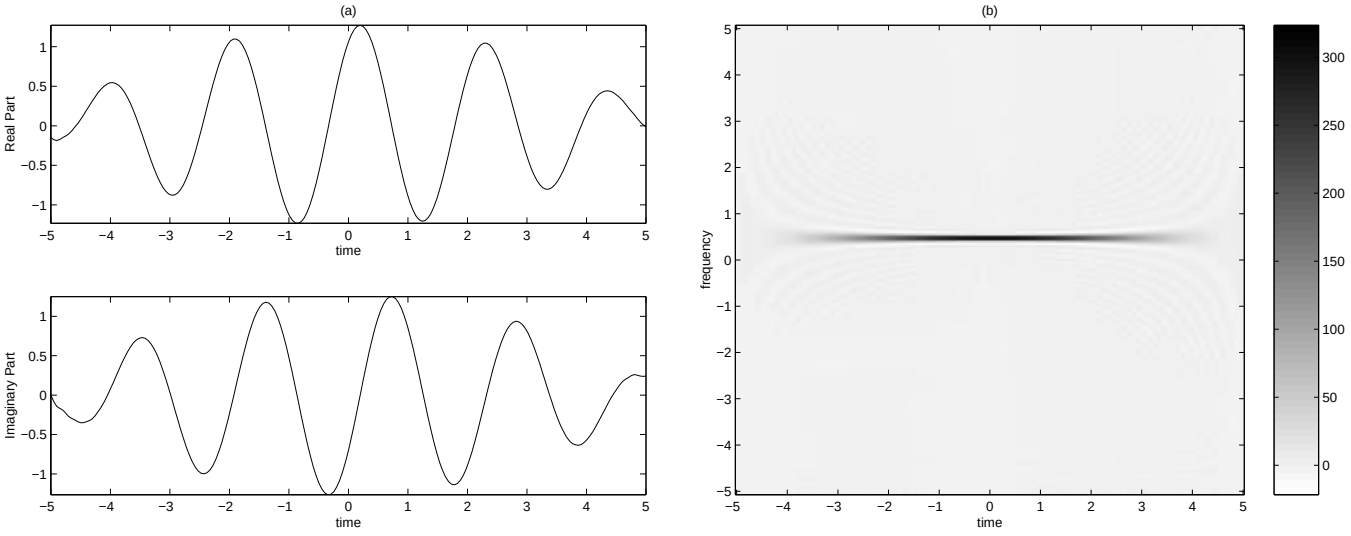

Figure 3.4: (a) The signal synthesized in the warped fractional Fourier transform domain by using the WD-based synthesis algorithm on the model time-frequency distribution given in Fig. 3.3 and (b) its Wigner distribution.

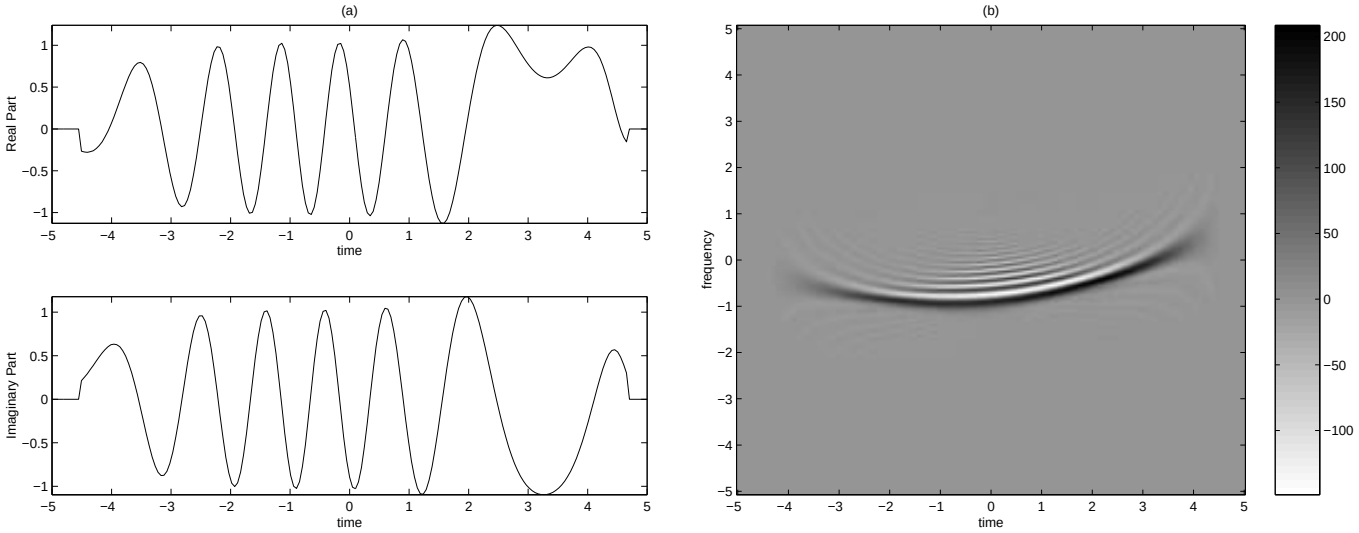

Figure 3.5: (a) The fractional Fourier transform representation of the synthesized signal, which is obtained by unwarping the signal in Fig. 3.4 (a) and (b) its Wigner distribution.

Algorithm 2 Proposed Synthesis Method

1. Mark some points on the spine.
2. Find the rotation angle ϕ, which gives a single valued instantaneous frequency.
3. Rotate the points on the spine by ϕ radians in the clock-wise direction. These rotated points $(t_i, \psi(t_i))$ specify the shape of the rotated spine. The other points on the rotated spine $(t, \psi(t))$ are computed by using the spline interpolator.
4. Compute the warping function $\zeta(t)$, its inverse $\zeta^{-1}(t)$ and the center frequency f_ψ by using the relations given in (3.3)-(3.6).
5. Get the amplitude modulator and instantaneous bandwidth parameters from the user, and construct a model time-frequency distribution around the center frequency f_ψ in the warped domain.
6. By using the WD-based synthesis algorithm synthesize the signal in the warped fractional Fourier transform domain.
7. Then by using the unwarping relations and the inverse fractional Fourier transformation compute the time domain representation of the designed signal.

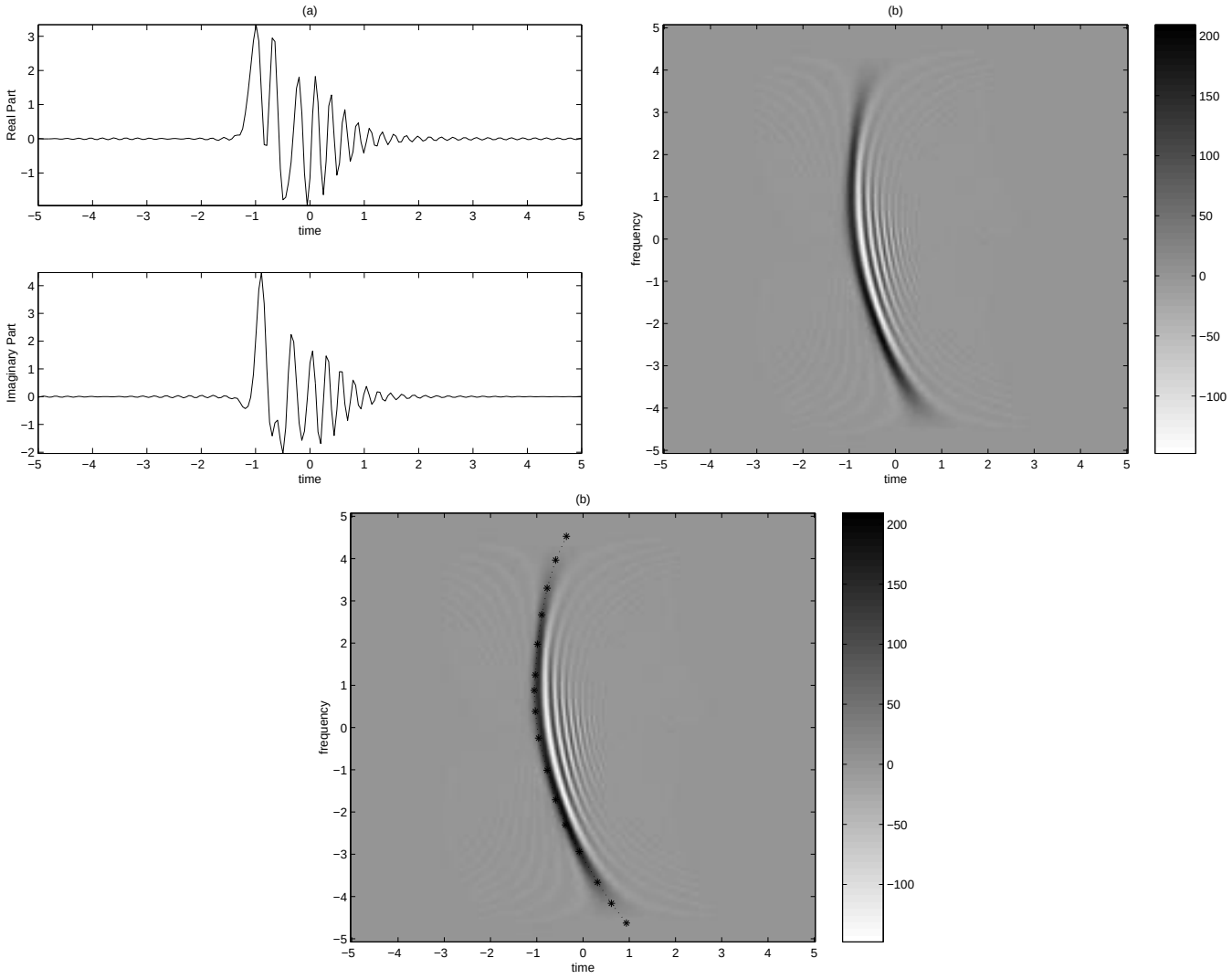

Figure 3.6: (a) The time domain representation of the synthesized signal, which is obtained by computing 0.909^{th} order FrFT of the signal in Fig. 3.5 (a), (b) its Wigner distribution (c) Wigner distribution overlaid with the spine.

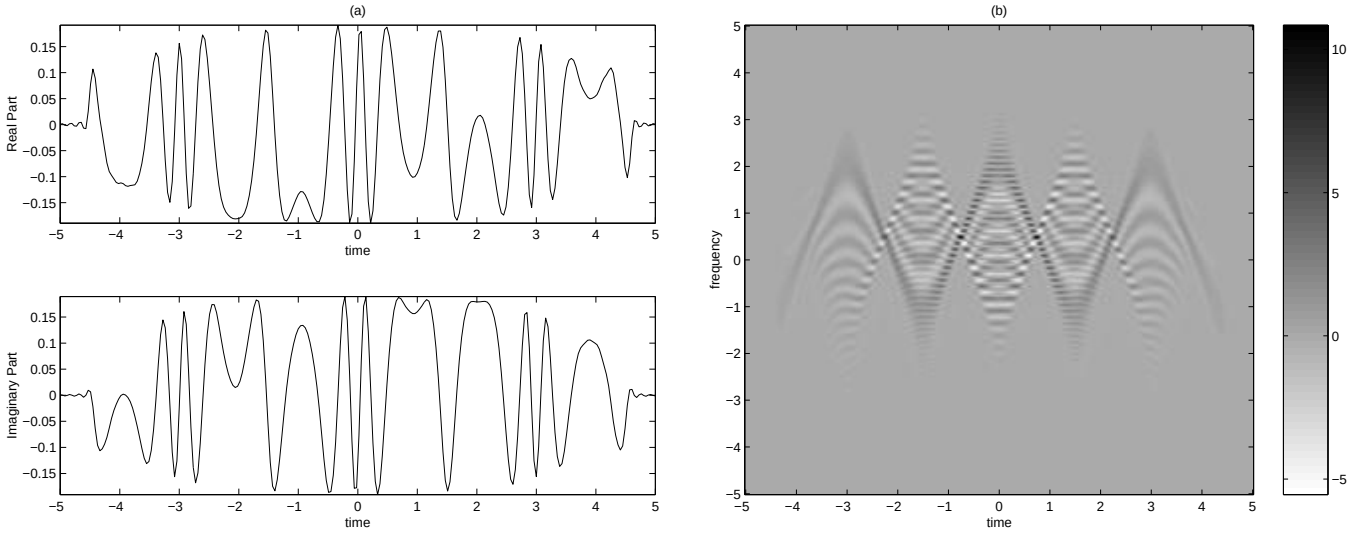

Figure 3.7: The simulation of the proposed synthesis method for the model Wigner given in Fig. 2.8 (a): (a) The signal synthesized by using the proposed synthesis method and (b) the Wigner distribution of the synthesized signal. The result is quite satisfactory in terms of fit to the desired region.

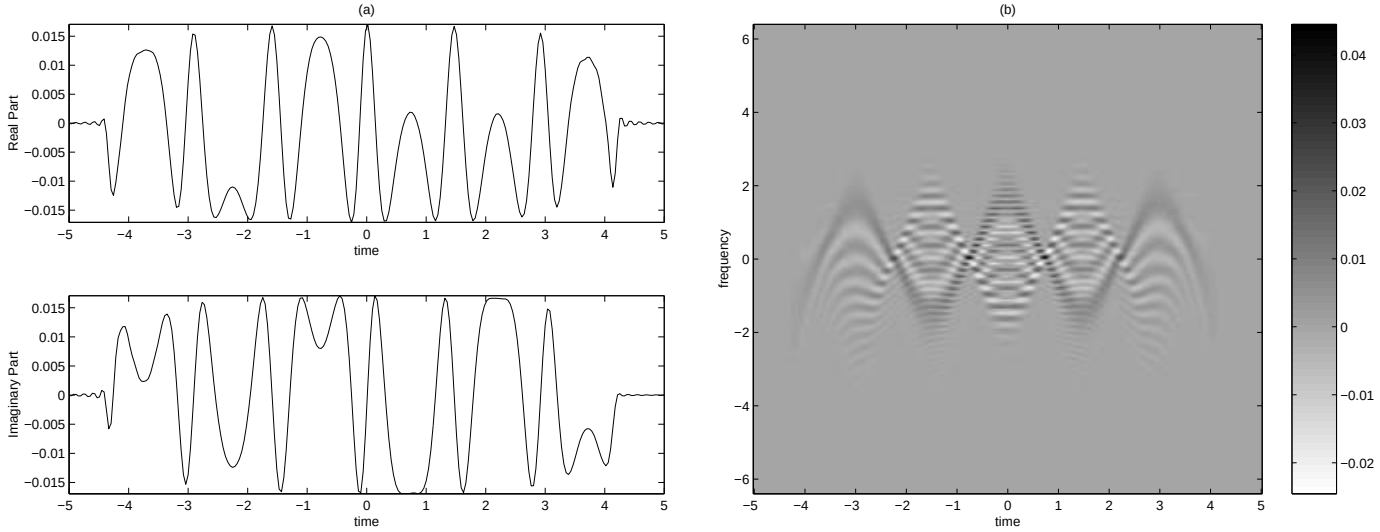

Figure 3.8: The simulation of the proposed synthesis method for the Wigner distribution given in Fig. 2.12 (b): (a) The signal synthesized by using the proposed synthesis method and (b) the Wigner distribution of the synthesized signal. The result is quite satisfactory in terms of fit to the desired region.

Chapter 4

Simulations

In this section we provide results of computer simulations using synthetic and real signals. In these simulation examples, the purpose is to compare the performance of the synthesis algorithms discussed in this paper on designing signals from time-frequency distributions. For synthetic signal a quadratic chirp is used. By real signals we refer to the signals which are found in nature such as the sounds of birds and whales or the sound of a police siren. The comparison method for the first type of simulations is chosen as the difference between the synthesized and actual signals, since the noise-free actual signal is available. For the real signals, the visual comparison of the designed and actual time-frequency distributions is preferred, since in this case the noise-free time domain representations of the actual signals are not available.

4.1 Synthetic Signals

In this section we compare the performance of WD-based, MWD-based and the proposed synthesis methods on a synthetic test signal. In this simulation the synthetic signal is chosen as

$$x(t) = e^{j\phi(t)} w(t) \qquad , \qquad -2 \leq t \leq 2 \quad , \tag{4.1}$$

where the non-linear phase of the signal is given by

$$\phi(t) = ct^3 + 2\pi t \quad , \tag{4.2}$$

and the envelope $w(t)$ of the non-linear phase term is chosen as shown in Fig. 4.1. The time-frequency representation of $x(t)$ changes significantly based on the value of the coefficient c. When $c = 0$, $x(t)$ has a linear time-frequency representation, and for $c > 0$ it has a parabolic time-frequency representation. As the value of c increases the curvature of the parabola increases. In Fig. 4.2 (a), Fig. 4.2 (c) the time domain signals and in Fig. 4.2 (b) and Fig. 4.2(d) the WD of $x(t)$ are given for $c = 0.2\pi$ and $c = 5.0\pi$ respectively. As it can be seen from these figures, as the value of the parameter c increases the inner interference terms occupy a larger portion of the time frequency plane.

In the simulation $N = 512$ uniformly spaced samples of the actual signal given in (4.1) are used to compute the discrete model WD. In the first part of the experiment the normalized errors of the algorithms are computed for various values of the parameter c in the interval $0.2\pi \leq c \leq 5.0\pi$. The normalized synthesis error for all of the four algorithms is computed as

$$\bar{e} = \frac{\int |x(t) - x_S(t)|^2 \, \mathrm{d}t}{\int |x(t)|^2 \, \mathrm{d}t} \quad , \tag{4.3}$$

where $x(t)$ is the actual signal and $x_S(t)$ is the synthesized signal. In the WD-based and MWD-based synthesis approaches, the model time-frequency distribution is chosen by removing the inner interference terms from the WD of the synthetic signal. For instance for $c = 2.6\pi$, the synthetic signal $x(t)$, its WD and the model WD are shown in Fig. 4.3 (a)-(c), respectively. In the simulations conducted for different values of the parameter c, the don't care region for the MWD-based synthesis algorithm is chosen similar to the one given in Fig. 4.3 (d) for the specific value of $c = 2.6\pi$. In the proposed synthesis method, the spine $\psi(t)$ of the signal is extracted from the model-WD given in Fig. 4.3 (c). Note that, in this simulation the spine is a single valued function of time which is strictly positive therefore there is no need for fractional Fourier transformation and frequency translation. In this simulation the model time-frequency distribution for the proposed synthesis method which should be given in the warped domain, is chosen as the WD of the warped signal $x_\zeta(t) \triangleq x(\zeta(t))$, where the warping function is computed from the spine $\psi(t)$ by using the relations given in (3.3)-(3.6) and $x(t)$ is the actual signal which is modeled as in (4.1). This selection of the model WD is necessary to make a fair comparison between the algorithms, since the other algorithms make use of the auto-term of the WD of the actual signal.

All of the algorithms are simulated for 13 different test signals which are obtained by changing the parameter c of the signal model given in (4.1) in the interval $[0.2\pi,\ 5\pi]$. The normalized errors of the algorithms computed by using (4.3) are given in Fig. 4.4 . As shown in Fig. 4.4 (a), the WD-based synthesis algorithm has a poor performance which worsens as the curvature of the auto-term increases.

The normalized errors for MWD-based FWD-based algorithms given in Fig. 4.4 (b) and Fig. 4.4 (c), respectively, confirms the better performance of these algorithms. However FWD-based algorithm produces much better results, since the normalized errors are on the order of 10^{-8} for this algorithm and on the order of 10^{-3} for the MWD-based synthesis algorithm.

To give more insight about the performance of the algorithms, the synthesis results for the value of $c = 2.6\pi$ are also documented. In Fig. 4.5 the synthesized signals overlaid with the actual signal, in Fig. 4.6 the Wigner distributions of the synthesized signals and in Fig. 4.7 the absolute synthesis error are given respectively. As it can be seen in Fig. 4.6, visually the auto-terms of the WDs of the synthesized signals are close to the model WD. However, the performance of the algorithms greatly vary when the synthesized signals are compared with the actual signal which is available in this simulation. For instance, in Fig. 4.7 (a) it is apparent that the synthesized signal cannot completely fit to the model for the WD-based synthesis algorithm, since the model WD given in Fig. 4.3 (c) lacks the inner interference terms. The modeling error increases considerably at the tails, where the auto-term in the model WD becomes curved. Therefore as the curvature of the model WD increases, the performance of the WD-based synthesis algorithm deteriorates.

As it can be seen in Fig. 4.7 (b) and Fig. 4.7 (c) both the MWD-based and proposed synthesis method produced more accurate signal designs than the WD-based synthesis algorithm. However the performance of the proposed synthesis method is much better than the MWD-based algorithm for this example.

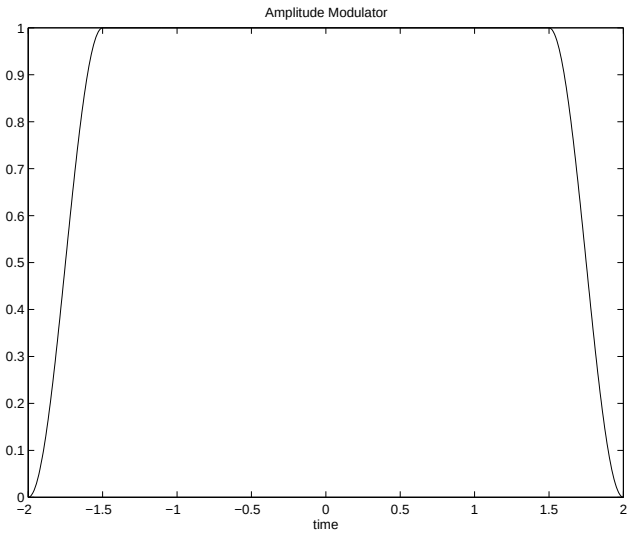

Figure 4.1: Simulation 1: The envelope $w(t)$ of the synthetic signal given by (4.1).

4.2 Results for Section 4.1

In Section 4.1, simulations were conducted on a quadratic chirp. The chirp had a parabolic support the curvature of which can be controlled by parameter c. To reflect the scenario of a typical signal design, the inner interference terms were removed manually while constructing the model from the Wigner distribution of the available time signal. The purpose of this set of simulations was to compare the synthesized signal with the original time signal and comment on the error.

First the normalized errors were obtained with respect to the change in parameter c in the interval $[0.2\pi,\ 5\pi]$, the results of which are given in Fig. 4.4. As c gets larger, the support of the inner interference terms occupy a larger space in time-frequency plane.

In WD-based synthesis the normalized error increased steadily with respect to c up to the order of %25 which is considerably high. This is because of the fact that as the support of the inner interference terms occupy a larger space, the lack of such terms in the model Wigner degrades the performance in fitting to the desired region. At a single point it showed a slight decrease which is not an exception but a result caused by errors coming from manually removing the inner interference terms. For the WD-based algorithm it can be concluded that it requires the modeling of interference terms for a successful synthesis result.

In MWD-based synthesis the normalized errors did not steadily increase and they were on the order of %0.1 which is an acceptable result. Again for some of the c values it became larger and for others it turned out to be considerably less. Such deviations arose from the errors coming from manually removing the inner interference terms in constructing the model and from manually constructing the don't-care mask. In other words at some c values, models and masks can be constructed unintentionally so that they are more likely to produce results closer to the original signal. For this algorithm it can be concluded that the lack of the inner interference terms in the model do not affect the performance but it is necessary to guess for the spread of such terms in constructing the don't-care mask. The need for the size of the interference terms is removed whereas there is still a requirement for their location. For this simulation example since the support of the model was simple, constructing a reliable don't-care mask was not a big problem but in more complicated scenarios definitely it will be more difficult and burdensome to determine the location of the inner interference terms and construct the don't-care mask and this will affect the performance.

In proposed synthesis method the warping is performed using the available time signal and the Wigner distribution of the warped signal is used as a model in the transformed signal domain. The reason for that is the other methods make use of the auto-term of Wigner distribution of the original signal which is not an expected case in signal design. Therefore to make a fair comparison between the algorithms, this model is specifically chosen as the Wigner of the warped signal which can still be constructed using (3.8). For this method, the normalized errors were on the order of $\%10^{-4}$ which is considerably less. The increase of error with respect to c is not related to the increase in interference term support but has to do with errors coming from the WD-based synthesis algorithm used in transformed signal domain and interpolation used in unwarping the synthesized signal. If the correct expression for the spine and correct warping relation is used, which are available from the analytical expression of the original signal and the sequence of warping-synthesis-unwarping operations are repeated, a similar increase in normalized error is observed as c increases. This behavior is shown in Fig. 4.2 When the correct values are used, the error coming from the warping part is considerably removed but there is still error coming from the synthesis and unwarping operations. Actually the misleading increase in the normalized error for the last three c values is directly caused by the tails of the quadratic chirp approaching to the aliasing boundary. For the proposed synthesis method it can be concluded that the requirement for the shape and location of the inner interference terms is removed. Furthermore, the performance is quite satisfactory and better than the existing approaches.

In the second set of simulations the synthesis error is obtained for a single value of $c = 2.6\pi$ and plotted with respect to time as shown in Fig. 4.7 . In WD-based and MWD-based synthesis methods, the absolute error increased at

the end-points of the quadratic chirp. This is because of the fact that the original signal is not bandlimited. It is an exponential which extends throughout the time-frequency plane, multiplied with an amplitude modulator which corresponds to convolution by a sinc function in the frequency variable. Therefore the error is concentrated at the falling edges of the amplitude modulator which accounts for the convolution by sinc. But in the proposed synthesis method, no such behavior is observed because the synthesis is performed in transformed signal domain where the model represents a bandlimited signal. The absolute error is also considerably less than the other methods.

4.3 Real Signal

The real data used in this section is conducted on the recorded sound of a Jamaican White-eyed Vireo bird [20]. In Fig. 4.9 (a) 13472 samples of the whole recording obtained at a rate of 16000 Hz is given. In this simulation, the analysis is conducted by using the 901 samples segment of the whole recording shown in Fig. 4.9 (b). The WD of this signal segment is computed as shown in Fig. 4.10 (a). In this plot, only the upper half part of the time-frequency plane is shown since the WD of a real signal is symmetric with respect to the time axis. In this simulation the model time-frequency distribution shown in Fig. 4.10(b) is obtained by removing the inner interference terms in Fig. 4.10(a) considerably. For the MWD-based synthesis algorithm, the don't care mask is chosen as shown in Fig. 4.11(a). The model time-frequency distribution for the proposed synthesis method is chosen as shown in Fig. 4.11 (b) in the warped time-frequency domain. Using these models, the synthesis algorithms discussed in this paper are simulated. The synthesized signals and their WDs are shown

in Fig. 4.12 and Fig. 4.13 respectively. In Fig. 4.12 (a) and Fig. 4.13 (a), it can be seen that the WD-based synthesis algorithm cannot model middle section of the model time-frequency distribution. The results for the MWD-based synthesis algorithm after 50 iterations are given in Fig. 4.12 (b) and Fig. 4.13 (b) respectively. In this simulation no energy penalty is used by setting $\gamma = 0$. By comparing the WD of the designed signal given in Fig. 4.13 (b) with the result of WD-based synthesis algorithm, it is clear that MWD-based synthesis algorithm produced more plausible results in this simulation. However the problems with this approach are its high computational complexity and the lack of research results on the optimum selection of the energy penalty factor. Finally, the results of the proposed synthesis method are given in Fig. 4.12 (c) and Fig. 4.13 (c) respectively. Not only the proposed synthesis method produced its results faster than the MWD-based algorithm, but it also produced a higher quality synthesis result.

4.4 Results for Section 4.3

In this simulation example, the performance of the algorithms were tested on a real signal that exists in nature. It was a song by Jamaican White-eyed Vireo bird. The comparison in this case is made through the Wigner plots of the resulting signals because the noise free time domain signal is not available. But time domain representations of the synthesized signals also provide valuable information about the quality of the designs. The main purpose of this simulation was to show that such type of signals with non-linear supports exist in nature. The WD-based synthesis algorithm failed to model the middle portion of the signal. Therefore it can be argued that the WD-based synthesis

algorithm is not a suitable method for such non-linear supports. MWD-based synthesis algorithm performed well but it requires the construction of don't-care mask which is troublesome. Actually here the don't-care mask is roughly chosen. Of course there are interference terms that will overlap some of the signal parts. But they are not easy to determine considering that we start from the cross term free model. In this case the performance of the MWD-basaed synthesis algorithm might be different if the user is more cautious in compactly determining the interference term structure. Therefore the performance is dependent to the don't-care mask. In proposed synthesis method, the model is again chosen as the Wigner distribution of the warped signal with the same reason as in Section 4.1. The synthesis result of proposed synthesis method was as satisfactory as the result of the MWD-based synthesis algorithm but it was obtained much more faster. Therefore this algorithm is more efficient than the MWD-based synthesis algorithm.

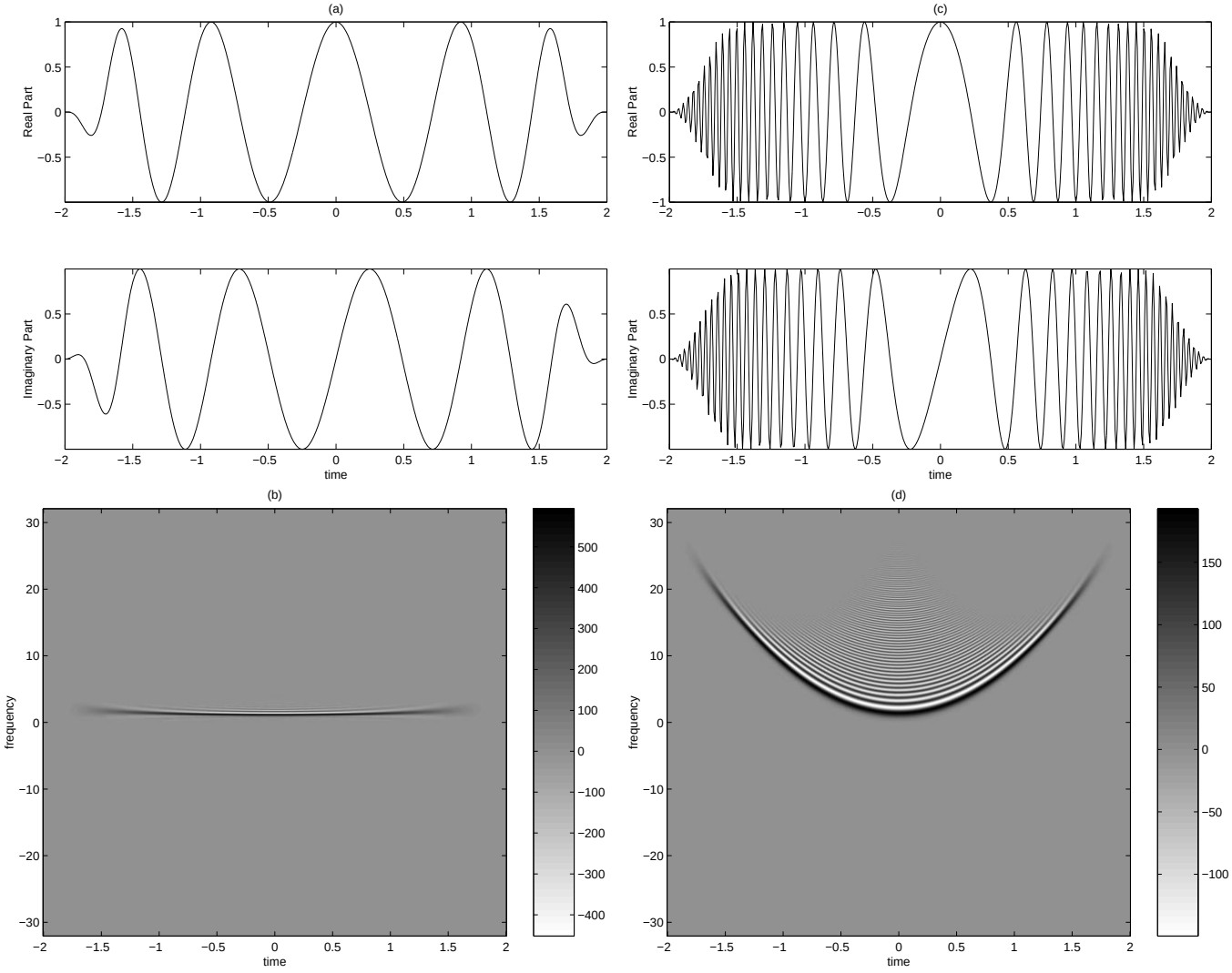

Figure 4.2: Simulation 1: (a) The time domain representation and (b) the WD of the signal whose model is given in (4.1) for $c = 0.2\pi$ and (c), (d) the corresponding plots for $c = 5\pi$. As the parameter c is increased from 0.2π to 5π the curvature of the parabolic support increases which increases the spread of the inner interference terms. This set up would be used in normalized error experiment.

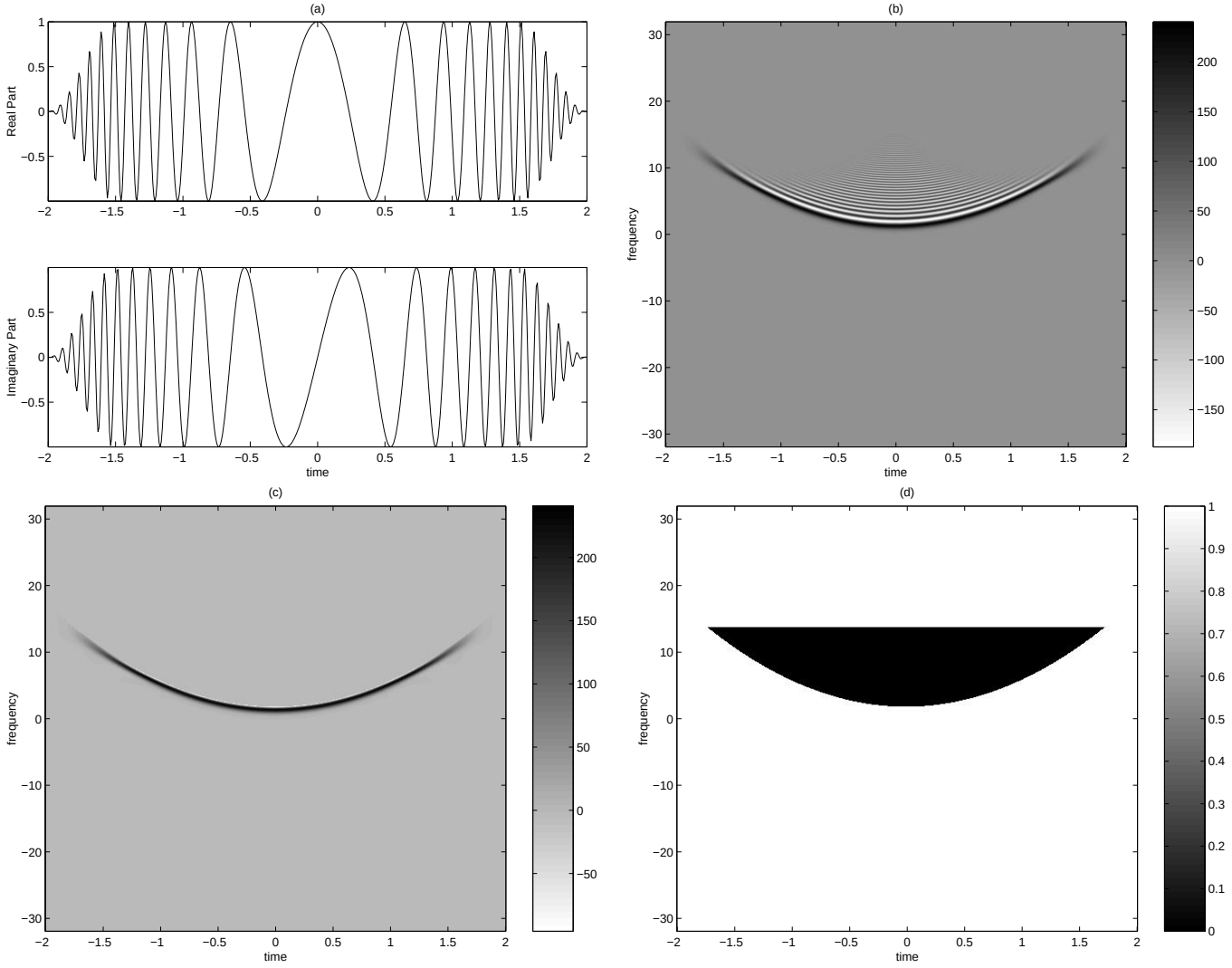

Figure 4.3: Simulation 1: (a) The time domain representation of the signal whose model is given in (4.1) for $c = 2.6\pi$ and (b) its Wigner distribution, (c) the model time-frequency distribution obtained by removing the interference terms of the WD given in (b) and (d) the don't-care region used for the MWD-based synthesis algorithm. This set up would be used in absolute error experiment which is conducted for a single value of c.

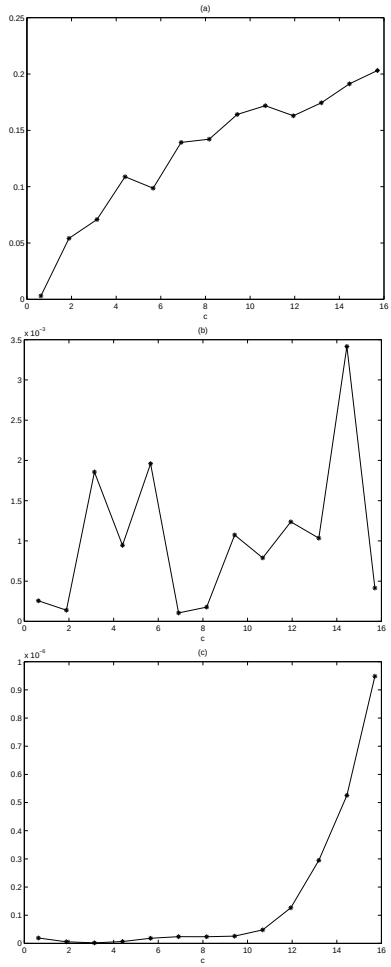

Figure 4.4: Simulation 1: Normalized error energies with respect to parameter c of (4.2) of the (a) WD-based (b) MWD-based (c) proposed synthesis methods computed by using the equation given in (4.3). The WD-based synthesis algorithm performed poorly which is on the order of %20 and the error increased with respect to the increase in the support of the inner interference terms. This is expected since model lacks interference term information. The MWD-based synthesis performed well which is on the order of %0.1 and is not affected from the spread of the inner interference terms. The proposed synthesis method performed very well which is on the order of $\%10^{-4}$. The misleading increase in the error as c gets larger has nothing to do with the increase in inner interference terms but related to the synthesis and interpolation errors which is also discussed in Section 4.2

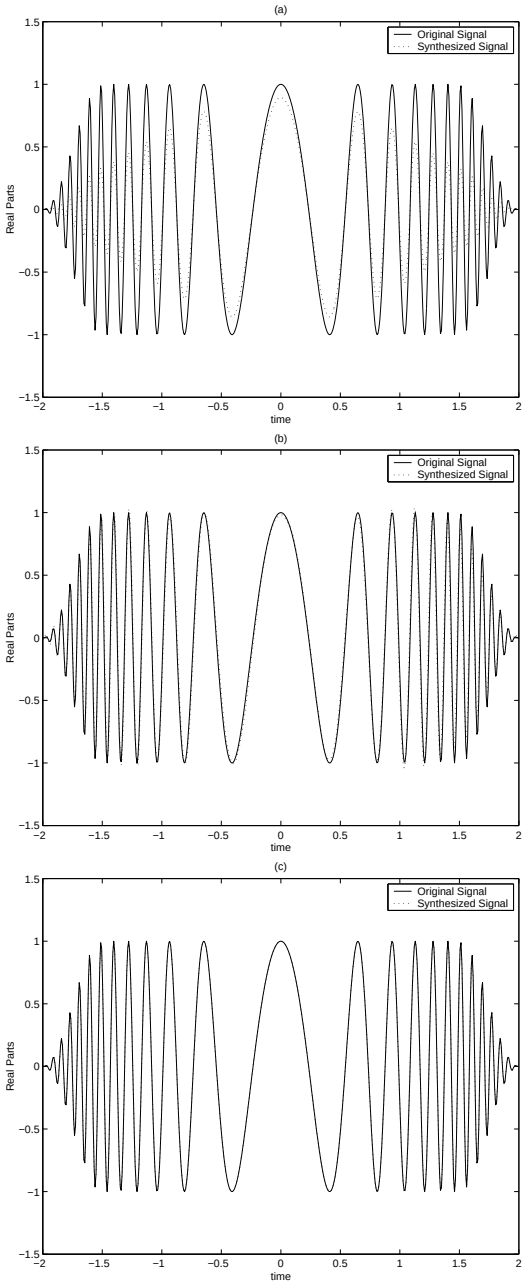

Figure 4.5: Simulation 1: The overlaid plots of the synthesized and the original signals for (a) WD-based, (b) MWD-based and (c) proposed synthesis methods. Designed signals for $c = 2.6\pi$. The WD-based synthesis algorithm performed poorly especially at the tails. MWD-based algorithm gave better results but at the tails the error again increased. The resulting signals are distinguishable from the original signal. FDW based-synthesis performed quite satisfactory results such that it is not distinguishable from the original signal.

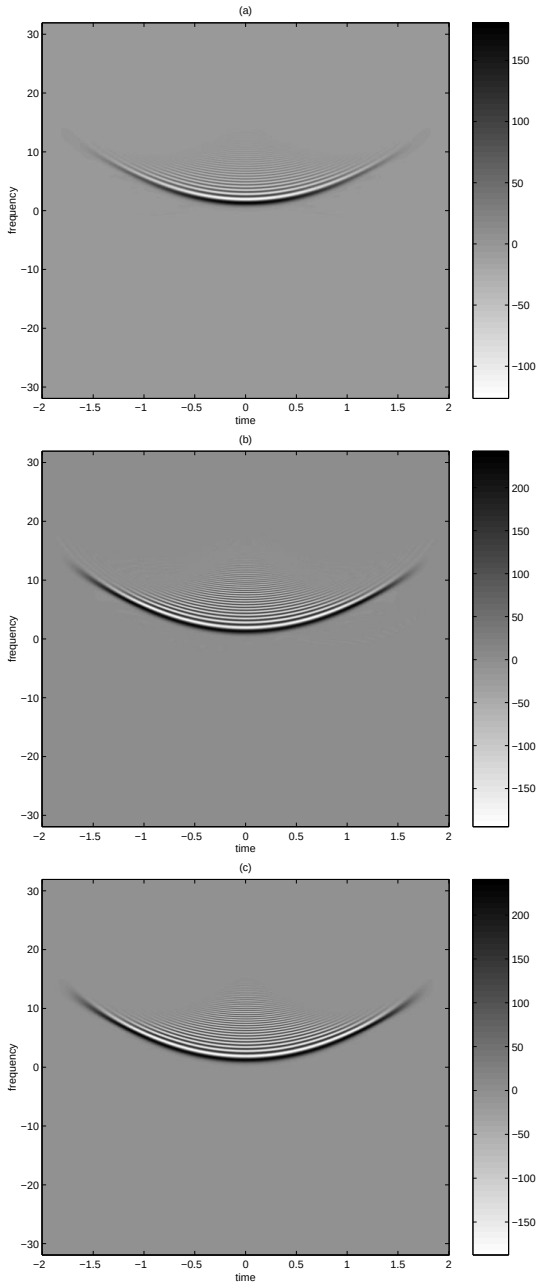

Figure 4.6: Simulation 1: The Wigner distribution of the signals synthesized for $c = 2.6\pi$ by using the (a) WD-based, (b) MWD-based and (c) Proposed Synthesis Method.

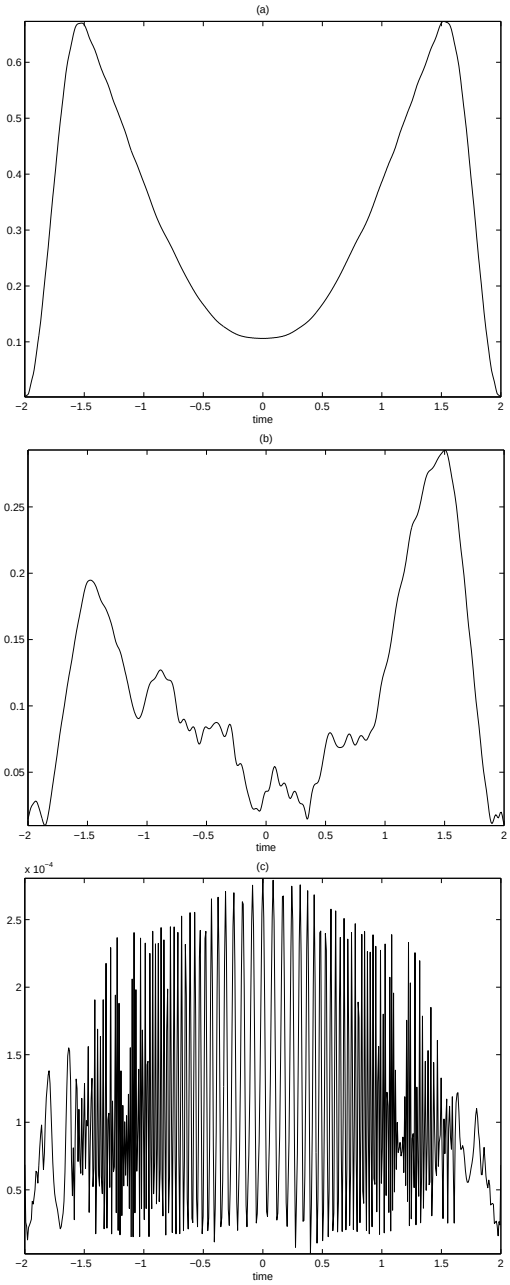

Figure 4.7: Simulation 1: The magnitude of the difference of the actual signal and the synthesis signals for $c = 2.6\pi$ obtained by using the (a) WD-based, (b) MWD-based and (c) proposed synthesis methods. WD-based and MWD-based methods suffered from the increase in error at the end-points of the chirp. This is related to the fact that these algorithms try to synthesize a signal which is not bandlimited. But proposed synthesis method performed very well because it used the model in the warped model which is bandlimited. This is discussed in Section 4.2 in detail.

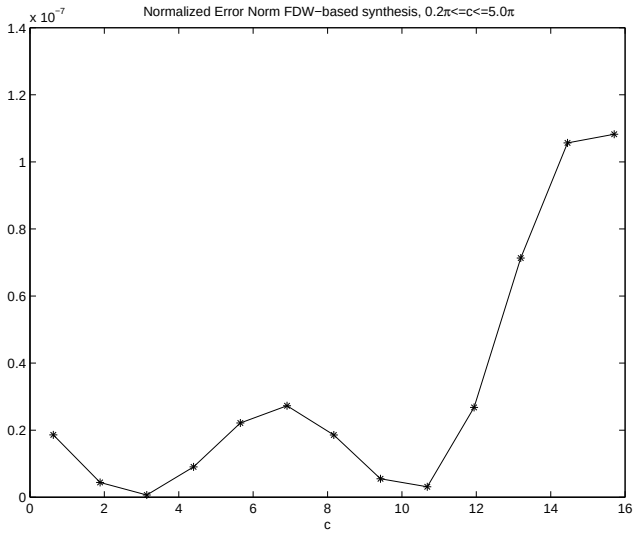

Figure 4.8: The normalized error in proposed synthesis method when the true spine and warping relation is used. Note the increase with respect to c even if the true values for the spine and warping relation are used. The increase in error is related to the synthesis errors and interpolation errors coming from unwarping operation. As c gets that large the chirp with the same number of samples, approach the aliasing region. Otherwise the increase has nothing to do with the inner interference terms since the synthesis is performed in transformed signal domain.

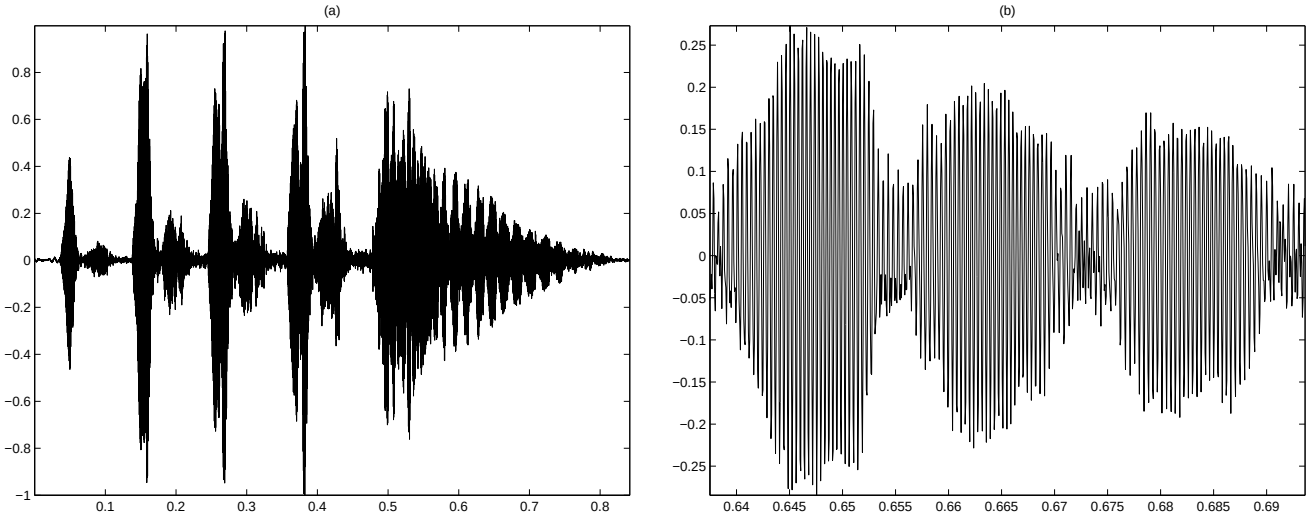

Figure 4.9: Simulation 2: (a) The whole recording of a Jamaican White-eyed Vireo bird sound and (b) the segment of this recording which is used in this simulation.

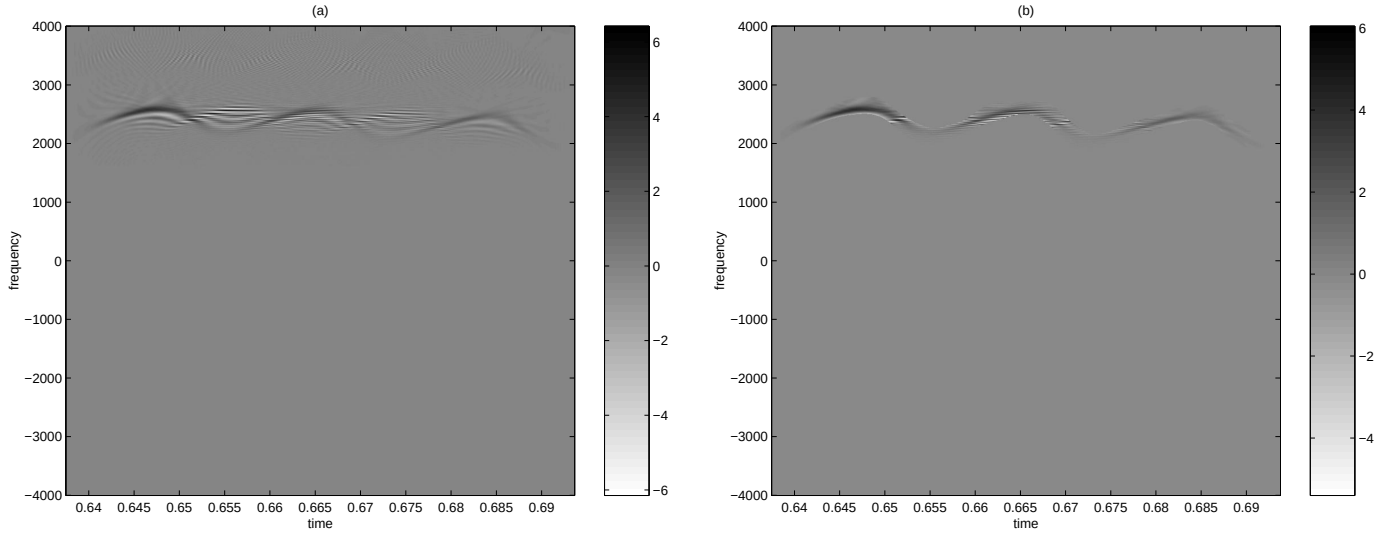

Figure 4.10: Simulation 2: (a) The Wigner distribution of jwev sound recording given in Fig. 4.9 and (b) the model time-frequency representation obtained by removing the interference terms of the WD given in (a). The symmetric part corresponding to negative frequencies is discarded and just the upper part is used as a model.

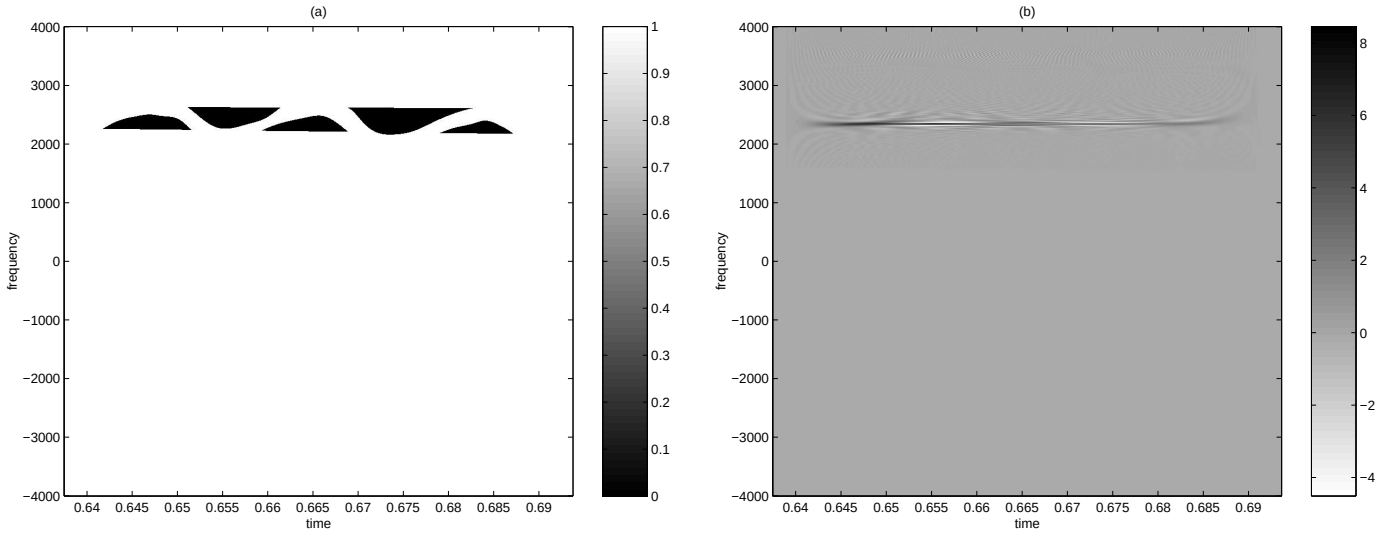

Figure 4.11: Simulation 2: (a) The don't care masked used in simulation of the MWD-based synthesis algorithm and (b) the model time-frequency distribution used by the proposed synthesis method in the warped time-frequency domain. The don't-care mask is chosen for obvious interference term locations which are inside the concavities of curved parts. Definitely there are more interference terms from different combinations of ramping portions going up and down. But they are not easy to specify therefore the most practical way is chosen.

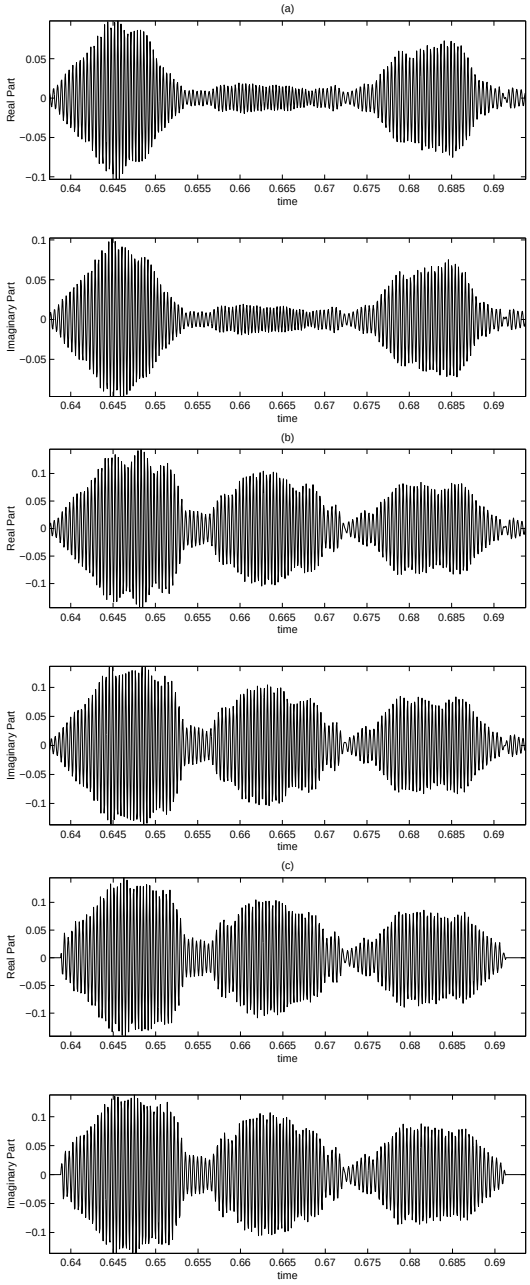

Figure 4.12: Simulation 2: The synthesized signals by using (a) the WD-based algorithm, (b) the MWD-based algorithm with no energy penalty and (e) the FDW based algorithm. The WD-based synthesis algorithm could not receive the middle portion due to lack of interference terms in the model Wigner. The MWD-based and proposed synthesis methods performed quite well. The proposed synthesis method produced its results faster.

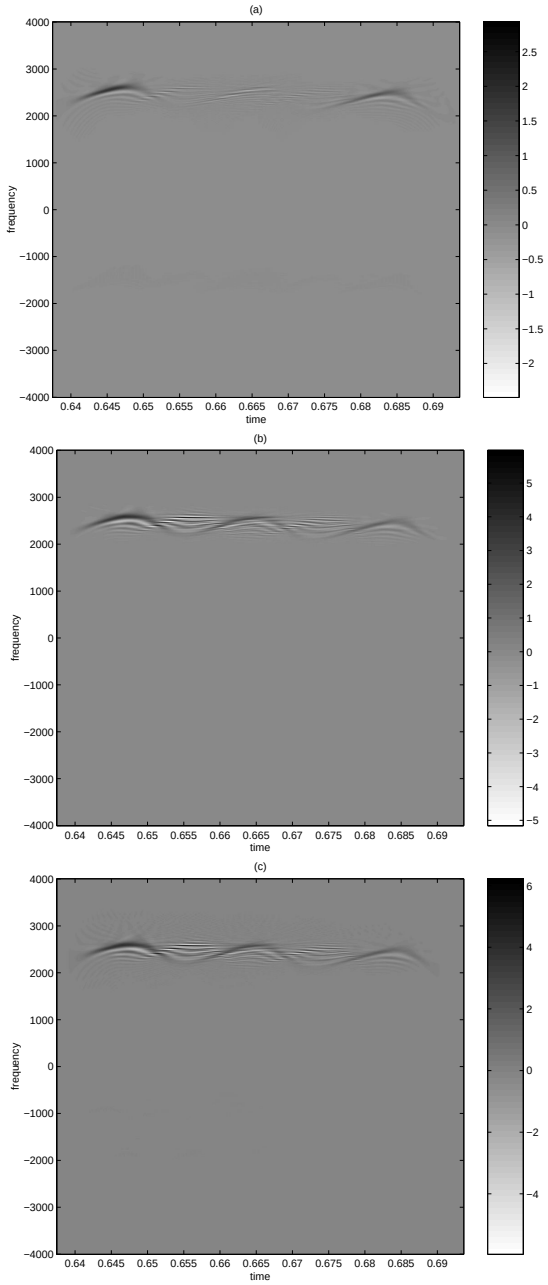

Figure 4.13: Simulation 2: The Wigner distributions of the synthesized signals designed by using (a) the WD-based algorithm, (b) the MWD-based algorithm with no energy penalty and (e) the FDW based algorithm.

Chapter 5

CONCLUSIONS

In this thesis, signal design in Wigner domain is investigated. First the two existing approaches are reviewed. They are the Wigner distribution based signal synthesis and the masked Wigner distribution MWD based signal synthesis algorithms. Their theoretical formulation is presented and their performance is tested on simulated examples. The weak and strong parts of these algorithms are discussed. In conclusion it is found that, WD-based synthesis method is preferable when the auto-term of the desired signal has linear support in time-frequency plane which corresponds to no or negligible inner interference terms. If the desired signal is expected to have significant levels of inner interference in Wigner domain, this algorithm is not suitable unless these interference terms are captured in the desired Wigner model. MWD-based synthesis is preferable when the inner interference terms do not overlap with the time-frequency support of the desired signal. By choosing the don't-care region to include most of the inner interference terms, the MWD-based synthesis can provide acceptable results. For complicated inner interference structure, determining the shape

of the don't-care mask can be very difficult and tedious. In addition to the difficulty in choosing the right mask, the complexity of the MWD-based synthesis algorithm is considerably higher because of its iterative computational procedure.

After discussing the existing approaches a novel signal design method is introduced. In this new method, the synthesis is performed in a transformed signal domain where the Wigner distribution of the desired signal has considerably less inner interference terms. Furthermore, the desired signal model is not directly specified in the original time domain. Instead, the desired signal model is specified in two stages. First the spine is entered in original time domain. Then a rotation angle which will enable a single valued spine is chosen. Using the samples of the rotated spine, the warping and unwarping relations as well as the center frequency where the warped signal would be concentrated is determined. After specifying these parameters in the original time domain, the spread of the desired signal energy is specified in the transformed signal domain. This is achieved by specifying the support and the amplitude of the signal energy around the spine. Using these parameters and the center frequency, the desired model Wigner is constructed in the transformed signal domain. Then the signal is synthesized using WD-based synthesis algorithm which is suitable since the desired signal has negligible inner interference terms in the transformed signal domain. After synthesizing a signal, it is transformed back to the original time domain using a generalized unwarping relation which is obtained as a cascade of unwarping operation and fractional Fourier transformation. The proposed method is quite practical and easy to use. Furthermore, because there is no iterations involved, it is considerably more efficient than any of the known techniques.

After presentation the new method, it has been tested and compared with the earlier approaches on simulated examples. The new method provided quite satisfactory results both in synthetic and real cases. The first set of simulations dealt with the synthetic signals. The analytic expression for such signals are available therefore the designed signals are compared with the original signals providing a precise design error. The normalized error is investigated with respect to the increase in the interference term support. It can be concluded that WD-based synthesis performed worse as the interference term support increases while MWD-based and proposed synthesis methods did not show such behavior. MWD-based synthesis requires a complicated don't-care mask. However, the proposed synthesis method does not require such a mask. It has been observed that the proposed method provided considerably better results than the MWD-based synthesis technique.

In the second set of simulations a real signal which has sinusoidal time-frequency domain is utilized in the comparison of MWD-based and the proposed synthesis techniques. The inner interference terms are removed by masking and the model is chosen as cross term free. The WD-based synthesis could not design the middle portion whereas the MWD-based and proposed synthesis methods performed quite satisfactory results. The don't-care mask is chosen so that the support of the outmost interference term is covered. In this case auto-term support is not interfered considerably with the don't-care region. But in general, it might not be the case. It could be necessary to enter a larger don't-care region if the clustering interference terms are not negligible. This will completely change the performance of the MWD-based synthesis algorithm.

In conclusion, the proposed signal design approach is applicable to all type of signals with localized time-frequency supports. Although it is in the class of the most efficient signal design techniques, the performance of the proposed design technique is superior to any of the known Wigner distribution based signal design techniques.

APPENDIX A

Proof of (2.10)

By inserting (2.6) and (2.4) into (2.8) and expanding the obtained expression, the cost function $J_D(x)$ can be written as

$$J_D(x) = T_s^2 \sum_n \int_{-1/2T_s}^{1/2T_s} |\sum_m (c^{\mathcal{M}}[n,m] - c_x[n,m]) e^{-j2\pi f m T_s}|^2 \, \mathrm{d}f \quad , \text{(A.1)}$$

$$= T_s^2 \sum_n \int_{-1/2T_s}^{1/2T_s} \sum_m \sum_{m'} (c^{\mathcal{M}}[n,m] - c_x[n,m]) \quad \text{(A.2)}$$

$$(c^{\mathcal{M}}[n,m'] - c_x[n,m'])^* e^{-j2\pi f (m-m')Ts} \, \mathrm{d}f \quad . \quad \text{(A.3)}$$

Then, by changing the order of integration and summation this expression can be simplified as

$$= T_s^2 \sum_n \sum_m \sum_{m'} (c^{\mathcal{M}}[n,m] - c_x[n,m])(c^{\mathcal{M}}[n,m'] - c_x[n,m'])^* \int_{-1/2T_s}^{1/2T_s} e^{-j2\pi f (m-m')T_s} \, \mathrm{d}f \quad ,$$

$$= T_s \sum_n \sum_m \sum_{m'} (c^{\mathcal{M}}[n,m] - c_x[n,m])(c^{\mathcal{M}}[n,m'] - c_x[n,m'])^* \delta[m-m'] \quad ,$$

$$= T_s \sum_n \sum_m |c^{\mathcal{M}}[n,m] - c_x[n,m]|^2 \quad , \quad \text{(A.4)}$$

where $\delta[m-m']$ is the unit sample function. By substituting (2.5) into (A.4), the cost function can be written as

$$J_D(x) = T_s(\sum_n \sum_m |c^{\mathcal{M}}[n,m]|^2 + \sum_n \sum_m |x[n+m]x^*[n-m]|^2 - \quad \text{(A.5)}$$

$$2\Re e\{\sum_n \sum_m x[n+m]^* x[n-m]c^{\mathcal{M}}[n,m]\}) \quad . \quad \text{(A.6)}$$

Since $x[n]$ is an half-band signal, by using Lemma 1 and Lemma 2 which are given below, it can be shown that the cost function in (A.5) can be written merely in terms of the even indexed samples of $x[n]$.

Lemma 2.

$$\sum_n \sum_m |x[n+m]x^*[n-m]|^2 = 2(\boldsymbol{x}_e^H \boldsymbol{x}_e)^2 \quad , \quad \text{(A.7)}$$

where $\boldsymbol{x}_e$ is the vector that contains the even indexed samples of $x[n]$.

Proof. To prove this lemma first some simple manipulations on the indices of the summations are done: □

$$\begin{aligned}
\sum_n \sum_m |x[n+m]x^*[n-m]|^2 &= \sum_n \sum_m |x[n+2m]x^*[n]|^2 \\
&= \sum_n \sum_m |x[2(n+m)]x^*[2n]|^2 + \\
&\quad \sum_n \sum_m |x[2(n+m)+1]x^*[2n+1]|^2 \\
&= \sum_n \sum_m |x[2m]x^*[2n]|^2 + \sum_n \sum_m |x[2m+1]x^*[2n+1]|^2 \\
&= [\sum_n |x[2n]|^2]^2 + [\sum_n |x[2n+1]|^2]^2 \\
&= (\boldsymbol{x}_e^H \boldsymbol{x}_e)^2 + (\boldsymbol{x}_o^H \boldsymbol{x}_o)^2 \quad ,
\end{aligned} \quad \text{(A.8)}$$

where $\boldsymbol{x}_o$ is the vector that contains the odd indexed samples of $x[n]$. To prove this lemma, it is left to show that $(\boldsymbol{x}_o^H \boldsymbol{x}_o)^2 = (\boldsymbol{x}_e^H \boldsymbol{x}_e)^2$. This result can be obtained be using the results given in Appendix C:

$$(\boldsymbol{x}_o^H \boldsymbol{x}_o)^2 = \sum_n |x_o[2n+1]|^2 \tag{A.9}$$

$$= \sum_n |x_e[n] * h[n]|^2 \quad , \tag{A.10}$$

where $h[n]$ is the all-pass filter given in (C.3). Then by using the Parsaval's relation, this expression can be written as

$$(\boldsymbol{x}_o^H \boldsymbol{x}_o)^2 = \int_{-1/2}^{1/2} |H(e^{j2\pi f}) X_e(e^{j2\pi f})|^2 \, \mathrm{d}f \quad , \tag{A.11}$$

in the discrete-time Fourier transform domain. Since $H((e^{j2\pi f})$ is an all-pass filter, this expression simplifies as

$$(\boldsymbol{x}_o^H \boldsymbol{x}_o)^2 = \int_{-1/2}^{1/2} |X_e(e^{j2\pi f})|^2 \, \mathrm{d}f \quad . \tag{A.12}$$

Thus by using the Parseval's relation once more, the derivation is completed:

$$(\boldsymbol{x}_o^H \boldsymbol{x}_o)^2 = \sum_n |x_e[n]|^2 \tag{A.13}$$

$$= (\boldsymbol{x}_o^H \boldsymbol{x}_o)^2 \quad . \tag{A.14}$$

Lemma 3.

$$\Re e\{\sum_n \sum_m x^*[n+m] x[n-m] c^{\mathcal{M}}[n,m]\} = x_e^H \tilde{\boldsymbol{D}} \, x_e \tag{A.15}$$

where $\tilde{\boldsymbol{D}}$ *is a matrix with entries* $\tilde{d}[m',n']$ *as given in* (A.22) *and* $\boldsymbol{x}_e$ *is the vector which contains the even indexed samples of* $x[n]$.

Proof. To prove this lemma, first we change the indices of summations:

$$\Re e\{\sum_n \sum_m x^*[n+m] x[n-m] c^{\mathcal{M}}[n,m]\} = 2\Re e\{\sum_n \sum_m x^*[n+2m] x[n] c^{\mathcal{M}}[n+m,m]\} \tag{A.16}$$

Then, we divide the summation over n by separating the odd and even indexed terms

$$\begin{aligned}\Re e\{\sum_n\sum_m x^*[n+m]x[n-m]c^{\mathcal{M}}[n,m]\} &= \Re e\{\sum_n\sum_m x^*[2n+2m]x[2n]c^{\mathcal{M}}[2n+m,m] \\ &\quad + \sum_n\sum_m x^*[2n+1+2m]x[2n+1]c^{\mathcal{M}}[2n+1+m,m]\} \qquad \text{(A.17)}\end{aligned}$$

and rearrange the indice of summations

$$\begin{aligned}\Re e\{\sum_n\sum_m x^*[n+m]x[n-m]c^{\mathcal{M}}[n,m]\} &= \Re e\{\sum_n\sum_m x^*[2m]x[2n]c^{\mathcal{M}}[n+m,m-n] \\ &\quad + \sum_n\sum_m x^*[2m+1]x[2n+1]c^{\mathcal{M}}[n+m+1,m-n]\} \ . \qquad \text{(A.18)}\end{aligned}$$

By using (C.2), the odd indexed samples in the above expression are written in terms of the even indexed samples:

$$\begin{aligned}\Re e\{\sum_n\sum_m x^*[n+m]x[n-m]c^{\mathcal{M}}[n,m]\} &= \Re e\{\sum_n\sum_m x^*[2m]x[2n]c^{\mathcal{M}}[n+m,m-n] \\ &\quad + \sum_n\sum_m(\sum_{m'} h^*[m-m']x^*[2m'])(\sum_{n'} h[n-n']x[2n'])c^{\mathcal{M}}[n+m+1,m-n]\} \\ &= \Re e\{\sum_{n'}\sum_{m'} x^*[2m']x[2n'](c^{\mathcal{M}}[n'+m',m'-n'] \\ &\quad + \sum_n^{!}\sum_m h^*[m-m']h[n-n']c^{\mathcal{M}}[n+m+1,m-n])\} \\ &= \Re e\{\sum_{n'}\sum_{m'} x^*[2m']x[2n']d[m',n']\} \ , \\ &= \sum_{n'}\sum_{m'} x^*[2m']\tilde{d}[m',n']x[2n'] \qquad \text{(A.19)}\end{aligned}$$

where $d[m',n']$ and $\tilde{d}[m',n']$ are defined as

$$\begin{aligned}d[m',n'] &= c^{\mathcal{M}}[n'+m',m'-n'] \qquad \text{(A.20)} \\ &\quad + \sum_n\sum_m h^*[m-m']h[n-n']c^{\mathcal{M}}[n+m+1,m-n] \qquad \text{(A.21)} \\ \tilde{d}[m',n'] &= d[m',n'] + d^*[n',m'] \ . \qquad \text{(A.22)}\end{aligned}$$

Note that, in matrix notation (A.19) can be written as

$$\Re e\{\sum_n \sum_m x^*[n+m]x[n-m]c^{\mathcal{M}}[n,m]\} = \boldsymbol{x}_e^H \tilde{\boldsymbol{D}}\, \boldsymbol{x}_e \quad , \tag{A.23}$$

where $\tilde{\boldsymbol{D}}$ is a matrix with entries $\tilde{d}[m',n']$ as given in (A.22) and $\boldsymbol{x}_e$ is the vector which contains the even indexed samples of $x[n]$. □

Thus based on these lemmas, (A.5) can be written as

$$J_D(x) = T_s \left[\sum_n \sum_m |c^{\mathcal{M}}[n,m]|^2 + 2(\boldsymbol{x}_e^H \boldsymbol{x}_e)^2 - \boldsymbol{x}_e^H \boldsymbol{D}\, \boldsymbol{x}_e \right] \quad . \tag{A.24}$$

APPENDIX B

Proof of Lemma 1

In this section, first show that $\sqrt{\lambda_1}/2\tilde{\boldsymbol{q}}_1$ is a local minimum of the cost function (2.1). This can be proved by showing that the Hessian $\mathcal{H}(x_e)$ of the cost function

$$\mathcal{H}(x_e) = 4\boldsymbol{I}\,||\boldsymbol{x}_e||^2 + 4\boldsymbol{x}_e\boldsymbol{x}_e^H - \boldsymbol{D} \quad , \tag{B.1}$$

evaluated at the stationary point $\sqrt{\lambda_1}/2\tilde{\boldsymbol{q}}_1$ of the cost function is a positive definite matrix, where the matrix $\boldsymbol{I}$ in (B.1) is the identity matrix.

By using the spectral expansion $\boldsymbol{D} = \sum_i \lambda_i \boldsymbol{q}_i \boldsymbol{q}_i^H$ in (B.1), it can be shown that the Hessian matrix at the stationary point $\sqrt{\lambda_1}/2\tilde{\boldsymbol{q}}_1$ takes the following form:

$$\mathcal{H}(\sqrt{\lambda_1}/2\tilde{\boldsymbol{q}}_1) = \lambda_1\boldsymbol{I} - \sum_{i\neq 1}\lambda_i\boldsymbol{q}_i\boldsymbol{q}_i^H \quad . \tag{B.2}$$

Then by using the spectral expansion $\boldsymbol{I} = \sum_i \boldsymbol{q}_i\boldsymbol{q}_i^H$ for the identity matrix (B.2) can be simplified as

$$\mathcal{H}(\sqrt{\lambda_1}/2\tilde{\boldsymbol{q}}_1) = \lambda_1\boldsymbol{q}_1\boldsymbol{q}_1^H - \sum_{i\neq 1}(\lambda_1 - \lambda_i)\boldsymbol{q}_i\boldsymbol{q}_i^H \quad . \tag{B.3}$$

Thus, the eigenvalues of $\mathcal{H}(\sqrt{\lambda_1}/2\tilde{\boldsymbol{q}}_1)$ are $\lambda_1,\ \lambda_1-\lambda_2, \lambda_1-\lambda_3, \ldots$ which are all positive, since $\lambda_1 > \lambda_i \quad , \quad i \neq 1$. Therefore the Hessian is a positive definite matrix when evaluated at $\sqrt{\lambda_1}/2\tilde{\boldsymbol{q}}_1$.

To show that $\sqrt{\lambda_1}/2\tilde{\boldsymbol{q}}_1$ is actually the global minimizer of the cost function in (2.1), it is enough to compute the cost function at the stationary points[1] $\sqrt{\lambda_1}/2\tilde{\boldsymbol{q}}_i$ and show that $J(\sqrt{\lambda_1}/2\tilde{\boldsymbol{q}}_1) < J(\sqrt{\lambda_1}/2\tilde{\boldsymbol{q}}_i)$, $\forall i \neq 1$. But this follows easily from (2.10), since $J(\sqrt{\lambda_i}/2\tilde{\boldsymbol{q}}_i)\sum_n \sum_m |c^M[n,m]|^2 - \lambda_i^2/8$.

[1]Since $J_D(x)$ is a differentiable function its global minimum will be either at one its stationary points or when its argument approaches to ∞. However, by analyzing the form of the cost function, it becomes apparent that when its argument approaches to ∞, the value of the cost function also approaches to ∞.

APPENDIX C

The Recovery of Odd Samples using Even Samples

Since the samples $x[n]$ of the continuous time signal $x(t)$ are obtained by sampling $x(t)$ at twice the Nyquist rate, the odd indexed samples of $x[n]$ can be exactly obtained from its even indexed samples. To show this result, we use the Shannon's sampling theorem which states that a halfband signal can be exactly and uniquely reconstructed from its even indexed samples as illustrated in Fig. C.1:

$$x[n] = \sum_m \frac{\sin(\frac{\pi}{2}(n-2m))}{\frac{\pi}{2}(n-2m)}\, x[2m] \quad . \tag{C.1}$$

Thus, the odd indexed samples of $x[n]$ can be written in terms of the even-indexed samples as

$$\begin{aligned} x_o[n] \triangleq x[2n+1] &= \sum_m \frac{\sin(\pi(n-m+1/2))}{\pi(n-m+1/2)}\, x[2m] \\ &= \sum_m h[n-m]x_e[m] \quad , \end{aligned} \tag{C.2}$$

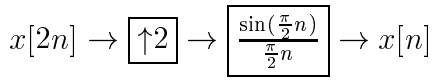

Figure C.1: Illustration of bandlimited interpolation by using the Shannon's sampling theorem.

where h[n] is an all-pass filter given by

$$h[n] = \frac{\sin(\pi(n+1/2))}{\pi(n+1/2)} \quad , \tag{C.3}$$

with Fourier transform $H(e^{j2\pi f}) = e^{j\pi f}$.

Bibliography

[1] L. Cohen, "Time–frequency distributions – A review," *Proc. IEEE*, vol. 77, pp. 941–981, July 1989.

[2] T. A. C. M. Claasen and W. F. G. Mecklenbrauker, "The Wigner distribution – A tool for time–time frequency signal analysis, Part I: Continuous–time signals," *Philips J. Res.*, vol. 35, no. 3, pp. 217–250, 1980.

[3] A. K. Özdemir and O. Arıkan, "A high resolution time frequency representation with significantly reduced cross–terms," *Proc. IEEE Int. Conf. Acoust. Speech Signal Process.*, vol. II, pp. 693–696, June 2000.

[4] W. Krattenhaler and F. Hlawatsch, "Time–frequency design and processing of signals via smoothed wigner distributions," *IEEE Trans. Signal Process.*, vol. 41, pp. 278–287, May 1993.

[5] F. H. e. W. F. G. Mecklenbrauker, *The Wigner distribution–theory and applications in signal processing.* Elsevier Science Publishers, 1997.

[6] L. Cohen, *Time–frequency analysis.* Prentice Hall, 1995.

[7] G. F. Boudreaux-Bartels and T. W. Parks, "Time–varying filtering and signal estimation using Wigner distribution synthesis techniques," *IEEE*

Trans. Acoust., Speech, and Signal Process., vol. ASSP–34, pp. 442–451, June 1986.

[8] F. Hlawatsch and W. Krattenhaler, "Bilinear signal synthesis," *IEEE Trans. Signal Process.*, vol. 40, pp. 352–363, Feb. 1992.

[9] F. Hlawatsch, A. H. Costa, and W. Krattenhaler, "Time–frequency signal synthesis with time–frequency extrapolation and don't–care regions," *IEEE Trans. Signal Process.*, vol. 42, pp. 2513–2520, Sept. 1994.

[10] F. Hlawatsch, "Interference terms in the Wigner distribution," in *Digital Signal Processing–84* (V. Cappellini and A. G. Constantidies, eds.), pp. 363–367, B. V. North Holland: Elsevier–Science Publishers, 1984.

[11] P. Flandrin, "Some features of time–frequency representations of multicomponent signals," *Proc. IEEE Int. Conf. Acoust. Speech Signal Process.*, vol. 3, pp. 41B.4.1–41B.4.4, 1984.

[12] T. A. C. M. Claasen and W. F. G. Mecklenbrauker, "The Wigner distribution – A tool for time–time frequency signal analysis, Part III: Rrelations with other time–frequency signal transformations," *Philips J. Res.*, vol. 35, no. 6, pp. 372–389, 1980.

[13] H. M. Ozaktas, Z. Zalevsky, and M. A. Kutay, *The Fractional Fourier Transform with Applications in Optics and Signal Processing.* John Wiley & Sons, 2001.

[14] L. B. Almedia, "The fractional Fourier transform and time–frequency representations," *IEEE Trans. Signal Process.*, vol. 42, pp. 3084–3091, Nov. 1994.

[15] A. K. Özdemir, L. Durak, and O. Arıkan, "High resolution time–frequency analysis based on fractional domain warping," accepted for publication in *Proc. IEEE Int. Conf. Acoust. Speech Signal Process.*, May 2001.

[16] M. H. Hayes, *Statistical DIgital Signal Processing and Modeling.* John Wiley & Sons, 1996.

[17] M. Unser, "Splines a perfect fit for signal and image processing," *IEEE Signal Processing Magazine*, vol. 16, pp. 22–38, Nov. 1999.

[18] H. M. Ozaktas and O. Aytur, "Fractional Fourier domains," *Signal Process.*, vol. 46, pp. 119–124, 1995.

[19] V. Namias, "The fractional order Fourier transform and its application to quantum mechanics," *J. Inst. Math. Appl.*, vol. 25, pp. 241–265, 1980.

[20] http://eebweb.arizona.edu/faculty/hopp/song.html